

1 **Technical Note: Lessons from and best practices for the** 2 **deployment of the Soil Water Isotope Storage System**

3 Rachel E. Havranek¹, Kathryn Snell¹, Sebastian Kopf¹, Brett Davidheiser-Kroll², Valerie Morris³, Bruce
4 Vaughn³

5 ¹Geological Sciences, University of Colorado Boulder, Boulder, 80303, USA

6 ²Thermo Fisher Scientific (Bremen) GmbH, Bremen, Germany

7 ³Institute of Arctic and Alpine Research, University of Colorado Boulder, Boulder, 80303, USA

8 *Correspondence to:* Rachel Havranek (rachel.havranek@colorado.edu)

9 **Abstract.** Soil water isotope datasets are useful for understanding connections between the
10 hydrosphere, atmosphere, biosphere, and geosphere. However, they have been underproduced
11 because of technical challenges associated with collecting those datasets. Here, we present the
12 results of testing and automation of the Soil Water Isotope Storage System (SWISS). The unique
13 innovation of the SWISS is that we are able to automatically collect water vapor from the critical
14 zone at a regular time interval and then store that water vapor until it can be measured back in a
15 laboratory setting. Through a series of quality assurance and quality control tests, we tested that
16 the SWISS is resistant to both atmospheric intrusion and leaking in both laboratory and field
17 settings. We assessed the accuracy and precision of the SWISS through a series of experiments
18 where water vapor of known composition was introduced into the flasks, stored for 14 days, and
19 then measured. From these experiments, after applying an offset correction to report our values
20 relative to VSMOW/SLAP, we assess the precision of the SWISS at $\pm 0.9\%$ and $\pm 3.7\%$ for $\delta^{18}\text{O}$
21 and $\delta^2\text{H}$, respectively. We deployed three SWISS units to three different field sites to
22 demonstrate that the SWISS stores water vapor reliably enough that we are able to differentiate
23 dynamics both between the sites as well within a single soil column. Overall, we demonstrate
24 that the SWISS retains the stable isotope composition of soil water vapor for long enough to
25 allow researchers to address a wide range of ecohydrologic questions.

26 **1 Introduction**

27 Understanding soil water dynamics across a range of environments and soil properties is
28 critical to food and water security (e.g. Mahindawansa et al., 2018; Quade et al., 2019; Rothfuss
29 et al., 2021); understanding biogeochemical cycles, such as the nitrogen and phosphorus cycles
30 (e.g. Hinckley et al., 2014; Harms and Ludwig, 2016); and understanding connections between
31 the hydrosphere, biosphere, geosphere and atmosphere (e.g. Vereeken et al., 2022). One
32 approach that can be used to understand water use and movement in the critical zone is the stable
33 isotope geochemistry of soil water (e.g. Sprenger et al., 2016; Bowen et al., 2019). Variations in
34 the stable isotope ratios of oxygen and hydrogen of soil water ($\delta^{18}\text{O}$, $\delta^2\text{H}$) track physical
35 processes like infiltration, root water uptake and evaporation. In particular, stable water isotopes
36 are useful for disentangling complex mixtures of water from multiple sources (e.g. Dawson and
37 Ehleringer, 1991; Brooks et al., 2010; Soderberg et al., 2012; Good et al., 2015; Bowen et al.,
38 2018; Gomez-Navarro et al., 2019; Sprenger and Allen 2020). Despite the long-recognized
39 utility of measuring soil water isotopes for understanding a range of processes (e.g. Zimmerman
40 et al., 1966; Peterson & Fry., 1987), soil water isotope datasets have been under-produced as
41 compared to groundwater and meteoric water isotope datasets (Bowen et al., 2019).

42 The primary barrier to producing soil water isotope datasets has been the arduous nature
43 of collecting samples. Historically, there are two primary methods for collecting soil water
44 samples: either digging a pit and collecting a mass of soil to bring back to the lab for subsequent
45 water extraction or via lysimeter. The former method disrupts the soil profile each time a sample
46 is collected, inhibiting the creation of long-term records of soil water isotopes. Lysimeters on the
47 other hand provide the means to collect multi-year soil water isotope datasets (e.g. Stumpp et al.,
48 2012, Zhao et al., 2013; Hinkley et al., 2014; Green et al., 2015; Groh et al., 2018), but the
49 choice of lysimeter can affect the portion of soil water (i.e. mobile vs. bound) that is sampled
50 (Hinkley et al., 2014; Sprenger et al., 2015) and the soil conditions that are sampleable (i.e.
51 saturation state). Soil water samples collected from both bulk soil samples and lysimeters often
52 require manual intervention at the time of sampling.

53 Building off of innovations in laser-based spectroscopy for stable isotope geochemistry,
54 the ecohydrology community developed a variety of in situ soil water sampling methods over the
55 last 15 years that enable the creation of high throughput, high precision analyses of soil water
56 isotopes (e.g. Wassenaar et al., 2008; Gupta et al. 2009; Rothfuss et al., 2013; Volkmann and
57 Weiler, 2014; Gaj et al., 2015; Oerter et al., 2016; Beyer et al., 2020; Kübert et al., 2020). These
58 methods have provided insights into a range of ecohydrologic questions from evaporation and
59 water use dynamics in managed soils (e.g. Oerter et al., 2017; Quade et al., 2018) to better
60 understanding where plants and trees source their water (e.g. Beyer et al., 2020). These
61 innovations have allowed researchers to ask new questions about ecohydrologic dynamics, but
62 current methods require field deployments of laser-based instruments. Field deployments are
63 technically possible and have been conducted successfully (e.g. Gaj et al., 2016; Volkmann et al.,
64 2016; Oerter et al., 2017; Quade et al., 2019; Künhammer et al., 2021; Seeger and Weiler., 2021;
65 Gessler et al., 2022), but require uninterrupted AC power, adequate shelter, as well as safe and
66 stable operating environments for best results. These prerequisites are often unavailable at many
67 field sites, especially in more remote locations and for longer sampling time frames. Given these
68 logistical constraints, these studies have mostly been done near the institutions performing those
69 studies. Spatial constraints limit the questions that researchers can ask about soil hydrology in
70 remote and traditionally understudied landscapes. For example, in the geoscience community
71 there is significant interest in improving the research community's understanding of how and
72 when paleoclimate proxies (e.g. stable isotope records from pedogenic carbonate, branched
73 glycerol dialkyl glycerol tetraethers, etc.) form in soils, because that informs our ability to
74 accurately interpret records from the geologic past. However, those projects commonly have
75 environmental constraints like soil type or local climate characteristics that may not be located
76 near institutions performing those studies. To be able to study a broader range of questions about
77 ecohydrology, there is a need for a system that is capable of autonomously collecting soil water
78 vapor for isotopic analysis in remote settings.

79 In this contribution, we report on the further development and testing of a field
80 deployable system called the Soil Water Isotope Storage System (SWISS). The SWISS was built
81 to be paired with ACCURELL PP V8/2HF vapor permeable probes that have been previously
82 tested for soil water isotope applications (Rothfuss et al., 2013; Oerter et al., 2017). Our system
83 uses three basic components to store water vapor produced by the vapor permeable probes: glass
84 flasks, stainless steel tubing and a flask selector valve (Fig. 1, Supplemental Table 1).
85 Previously, we demonstrated through a series of lab experiments that the glass flasks used in the
86 SWISS units can reliably store water vapor for up to 30 days (Havranek et al., 2020). That proof-
87 of-concept study demonstrated that the flasks retain original water isotope values, but the

88 laboratory system was not field deployable and did not have customizable automation. Here, we
89 present a fully autonomous, field-ready system that has been tested under both laboratory
90 conditions and field conditions, including development and testing of a solar-powered, battery
91 backed automation system that enables pre-scheduled water vapor sampling without manual
92 intervention in remote field locations.

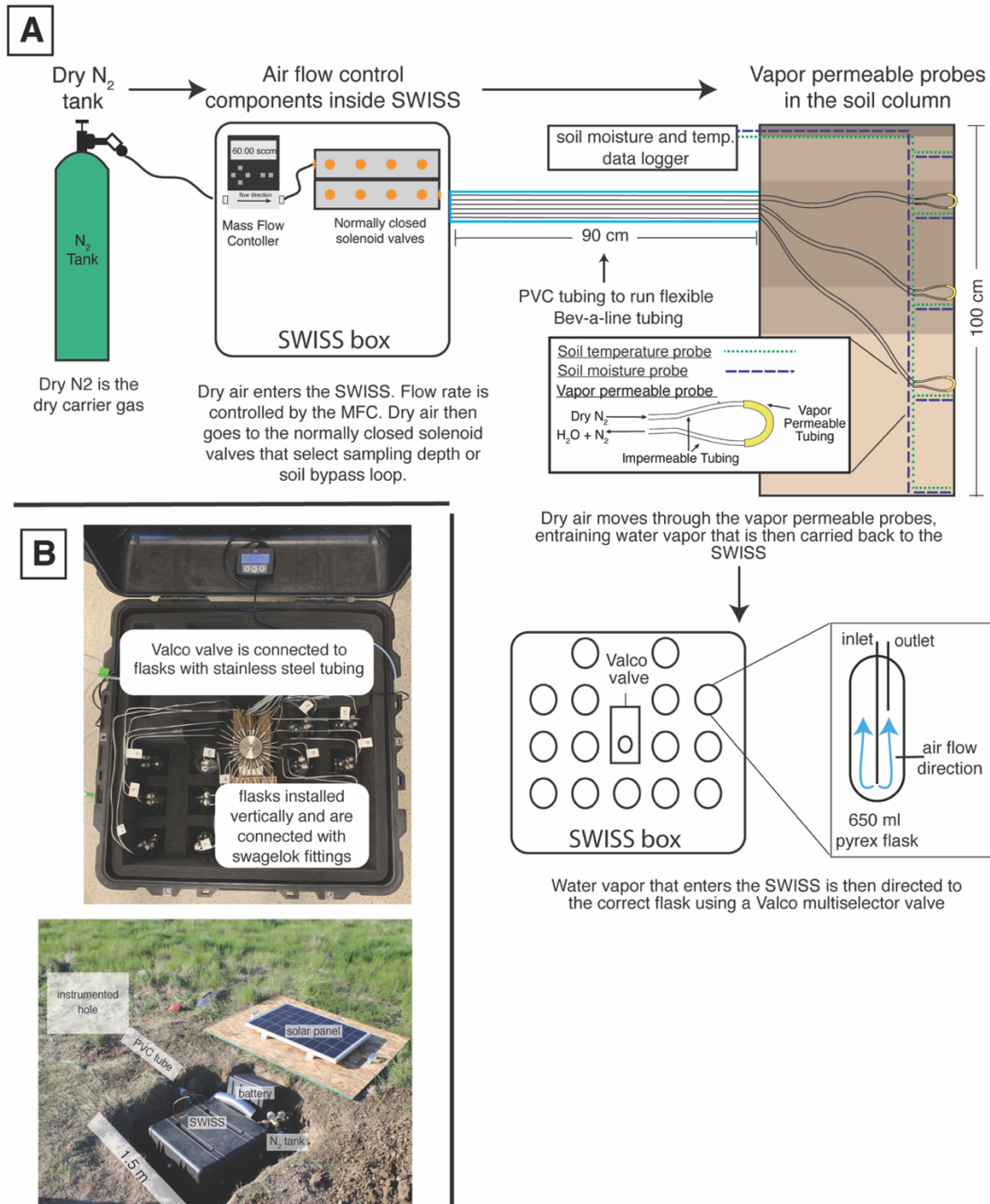
93 To test the accuracy and precision of the SWISS, we completed quality assurance and
94 quality control (QA/QC) tests. Here, we demonstrate the viability of this system under field-
95 conditions through two field suitability experiments. In addition, we sampled three different field
96 sites to show that the automation schema works on a monthly timescale and that the system
97 preserves soil water vapor isotope signals with sufficient precision to distinguish between three
98 different field settings and vertical profile differences.

99 **2 Field Sites**

100 ***2.1 Site Set-Up***

101 At each site we dug two holes; figure 1 shows the field-setup employed at all of our field
102 sites. One hole was instrumented with soil moisture and temperature data loggers at 25 cm, 50
103 cm, 75 cm, and 100 cm depths, as well as the water vapor permeable probes at 25 cm, 50 cm and
104 75 cm depths (Fig 1A). We deployed all probes >9 months before the first samples were
105 collected to allow the soil to settle and return to natural conditions as much as possible. This
106 timeframe was longer than other studies (e.g. Kübert et al., 2020) and included infiltration of
107 spring and early summer precipitation. During probe deployment we took care to retain the
108 original soil horizon sequence and horizon depths as much as possible. In the second hole, we
109 stored the SWISS unit, dry nitrogen tank, and associated components to power the SWISS (Fig
110 1B). The water vapor probes, which connected to the SWISS units with Bev-A-Line
111 impermeable tubing, were run through a PVC pipe buried at approximately 15 cm depth. We ran
112 the impermeable tubing underground to limit the effect of diurnal temperature variability on the
113 impermeable tubing to prevent condensation as water travels from the relatively warm soil to the
114 SWISS.

115



116
 117 **Figure 1.** A) The sampling flow path. To sample soil water, dry nitrogen is regulated at a specific rate
 118 using a mass flow controller, and then directed to one of the three sampling depths, or the soil bypass loop
 119 using a set of solenoid valves. Both the mass flow controller and solenoid valves are housed inside the
 120 SWISS. Once directed to the correct sampling depth, dry nitrogen is carried to the vapor permeable
 121 probes via gas impermeable tubing that is buried approximately 15 cm depth. After passing through the
 122 vapor permeable probe, the entrained soil water vapor is carried back to the SWISS where it is directed to
 123 the correct flask using a Valco multiselector valve. B) Photos of a built-out SWISS and the layout of a
 124 field site. Each of the system components (solar panel, battery, N_2 tank, SWISS, PVC tube) are labeled, in
 125 addition to the location of the instrumented hole in which all of the probes are buried. The hole which
 126 houses the SWISS, power, and N_2 tank is approximately 1.5 m wide.

127 **2.2 Site descriptions**

128 We deployed the SWISS at three field locations: Oglala National Grassland, Nebraska,
129 USA; Briggsdale, Colorado, USA; and Seibert, Colorado, USA. The Oglala National Grassland
130 site (Lat: 42.9600/Long: -103.5979/Elev: 1117 m) is located in northwestern Nebraska, USA in a
131 cold semi-arid climate. The soil at this site is described as an Aridisol with a silt-loam texture. It
132 is part of the Olney series (Natural Resources Conservation Service, 2022). The Briggsdale site
133 (Lat: 40.5947/Long: -104.3190/Elev: 1480 m) is located in northeastern Colorado, USA in a cold
134 semi-arid climate. The soil at this site is described as an Alfisol with a loamy sand - sandy loam
135 texture. It is part of the Olne series (Natural Resources Conservation Service, 2022). Long term
136 meteorological data from the Briggsdale site is available from the co-located CoAgMet site
137 (CoAgMet, Colorado Climate Center). The Seibert site (Lat: 39.1187/Long: -102.9250/Elev:
138 1479 m) is located in eastern Colorado, USA in a cold semi-arid climate. The soil at this site has
139 been described as an Alfisol, that has a sand loam texture in the top 50 cm of the profile, and a
140 silt loam texture between 50 - 100 cm. It is part of the Stoneham series (Natural Resources
141 Conservation Service, 2022). Long term meteorological data from the site is available from the
142 co-located CoAgMet site (CoAgMet, Colorado Climate Center).

143 **3 Materials**

144 **3.1 SWISS Hardware components**

145 In each SWISS there are 15 custom made ~650 ml flasks. These flasks are designed
146 similarly to those used for other water vapor applications. For example, a similar flask is
147 currently used in an unmanned aerial vehicle to collect atmospheric water vapor samples for
148 stable isotope analysis (Rozmiarek et al., 2021). The flasks have one long inlet tube that extends
149 into the flask almost to the base, and one shorter outlet tube so that vapor exiting the flask is well
150 mixed and representative of the whole flask (Fig. 1A). The large flask volume is advantageous
151 because there is a low glass surface area to volume ratio, and therefore we are able to reliably
152 measure vapor from the flasks on a cavity ring down spectroscopy (CRDS) instrument without
153 interacting with vapor bound to the flask walls. The 15 glass flasks are connected to a 16-port,
154 multi-selector Valco valve. We chose to use a Valco valve because these have previously been
155 shown to sufficiently seal off sample volumes for subsequent stable isotope analysis (Theis et al.,
156 2004). The valve and flasks are connected by 1/8 inch stainless steel tubing and stainless steel
157 1/4 inch to 1/8 inch union Swagelok fittings; we use PTFE ferrules on the glass flasks with the
158 Swagelok fittings. The first port of the Valco valve is 1/8 inch stainless steel tubing that serves as
159 a flask bypass loop, which enables flushing of either dry air or water vapor through the system
160 without interacting with a flask. All components are contained in a 61 cm x 61 cm x 61 cm
161 Pelican case (Pelican 0370) with three layers of Pick n' Pluck foam and convoluted foam
162 (Pelican Products Inc., Torrance, Ca, USA). This case is thermally insulated and provides
163 enough protection to safely transport the SWISS by vehicle to field sites.

165 **3.2 Soil Probes**

166 There are three components for the collection and analysis of soil water vapor: vapor
167 permeable probes, soil temperature loggers, and soil moisture sensors (Fig 1B, Supplemental
168 Table 1).

169 Here, we use a vapor permeable membrane (Accurrell PP V8/2HF, 3M, Germany) that
170 was first tested for soil water isotope applications by Rothfuss et al., (2013). This method works
171 by flushing dry nitrogen (or dry air) through the vapor permeable membrane, creating a water

172 vapor concentration gradient from inside the probe to the soil, thus inducing water vapor
173 movement across the membrane. Water vapor is then entrained in the dry nitrogen and flushed to
174 either a CRDS system or into a storage container. We opted to use this tubing because it has been
175 shown to deliver reliable data over time (i.e. Rothfuss et al., 2015; Oerter et al., 2019; Kübert et
176 al., 2020; Seeger and Weiler, 2021; Gessler et al., 2021), and it is easy to use and customize to
177 individual needs (Beyer et al., 2020; Kübert et al., 2020). We previously observed that variability
178 in the length of the vapor permeable tubing can lead to systematic offsets in the stable isotope
179 composition of measured waters that arise from variability of vapor permeable tube surface area
180 (Havranek et al., 2020). Therefore, we were careful to construct all probes such that the length
181 of the Accurrell vapor permeable tubing was 10 cm long, and the impermeable Bev-A-Line IV
182 connected on each side of the vapor permeable tubing was 2 m long. We cut the Bev-A-Line
183 connections to identical lengths to control for memory effect and to treat all samples identically.
184 We also constructed the vapor permeable probes to be used in the lab setting for standards in an
185 identical fashion.

186 Soil temperature loggers (Onset HOBO MX2201), used for applying a temperature
187 correction to all soil water vapor data and to provide key physical parameters of the soils for
188 other goals beyond this study, were buried at the same depths as the vapor permeable probes.
189 Soil moisture sensors (Onset S-SMD-M005) were also buried at the same depths as the vapor
190 permeable probes.

191

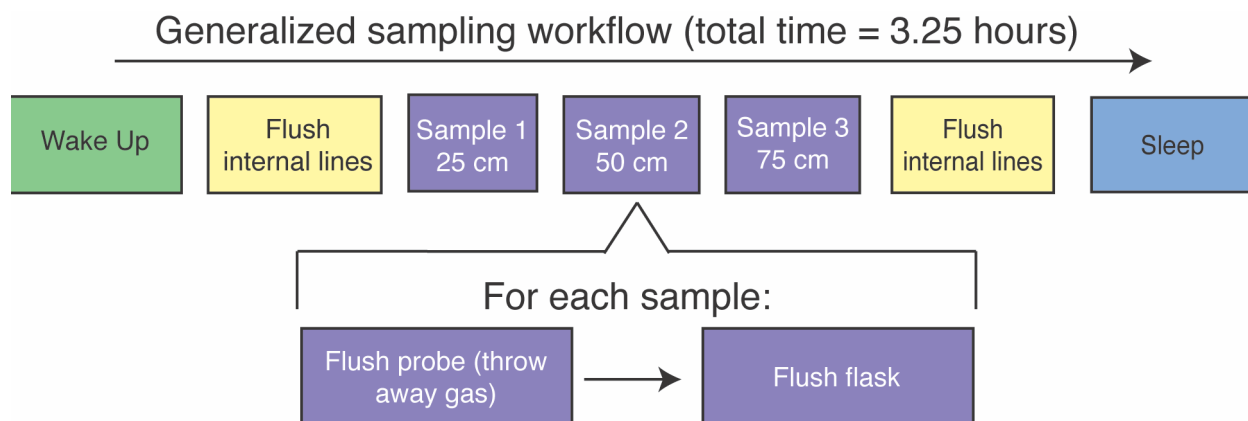
192 **3. 3 Automation components, code style, and remote setting power**

193 The philosophy behind the automation of the SWISS was to make it as easy to reproduce
194 as possible, and as flexible as possible to meet different users' sampling needs. We therefore use
195 widely available hardware components and electronics parts; for each product there are
196 numerous alternatives which should be equally viable and could be swapped to better meet each
197 user's needs. In an effort to make our system as accessible and customizable as possible for the
198 scientific community, all automation code is completely open source and will continue to be
199 refined for future applications and hardware improvements. We note that all code is provided as-
200 is and should be tested carefully for use in other experiments.

201 The overall sampling scheme used in this paper is described in figure 2 and table 1. Our
202 experimental goal was to create a time series of soil water vapor data from three discrete
203 sampling depths (25 cm, 50 cm, 75 cm). Prior to sampling any soil water vapor, we bypassed the
204 soil probes and flushed the lines within the SWISS. Then, at the start of sampling for each depth,
205 we also flushed the water vapor probe to remove condensation or 'old' water vapor. The gas
206 from both of those steps was expelled via the flask bypass loop. Each soil depth was then
207 sampled for 45 minutes by flushing through the next flask designated in the sequence.

208 Supplemental figure 1 shows the components of the automation system. To automate and
209 program the sampling scheme, we used: (1) a microcontroller to run the automation script; (2) a
210 coin-cell battery powered real time clock so that the microcontroller was always capable of
211 keeping track of time through power losses, and therefore maintain the sampling schedule; (3) an
212 RS-232 to TTL converter for serial communication with the Valco valve; (4) solenoid valves that
213 were used to control which depth was being sampled and the associated direct current (VDC)
214 power relay; (5) a mass flow controller used to control the rate at which dry nitrogen (1 ppm
215 H₂O) is flushed through the probes; and (6) a power relay used to power the Valco valve and
216 mass flow controller. All parts are described in detail in Supplemental Table 2.

217



218
219 **Figure 2.** Flow chart of the instrument schedule used for sampling during all field experiments.
220

221 **Table 1.** Description of soil water sampling steps

Code Step	Wake-up	Flush internal lines	Flush depth 1	Sample depth 1	Flush depth 2	Sample depth 2	Flush depth 3	Sample depth 3	Flush internal lines	sleep
time (minutes)	1	15	10	45	10	45	10	45	15	1
Valco valve position	flask bypass	flask bypass	flask bypass	2, 5, 8, 11, or 14	flask bypass	3, 6, 9, 12, or 15	flask bypass	4, 7, 10, 13, or 16	flask bypass	flask bypass
solenoid valve position	none	soil bypass	25 cm	25 cm	50 cm	50 cm	75 cm	75 cm	soil bypass	none

222
223 In a remote setting, the SWISS units are powered using the combination of a 12 volt
224 deep-cycle battery with a 12VDC, 100 watt solar panel that is used to charge the battery. The
225 solar panel is mounted to a piece of plywood that covers the hole where the SWISS is deployed
226 (note, the hole is uncovered in Fig. 1B for illustrative purposes). We opted for this setup because
227 the underground storage of all parts of the system creates a discreet field site that attracts
228 minimal attention from other land users, and helps reduce exposure to temperature and
229 precipitation extremes. In the field, we used a 12VDC-120VAC power inverter to provide simple
230 plug and play power for the Valco valve and mass flow controller. This simple combination was
231 suitable for summertime in the Western U.S. where there are many hours of direct sunlight, and
232 the solar panel was able to easily charge the 12V battery. This setup may need to be adjusted
233 based on location and desired sampling time. Like the automation system, there are many
234 commercial options available for products, and they can be easily adjusted for users' needs;
235 example parts are described in detail in Supplemental Table 2. We also note that in areas where it
236 is possible to plug into a power grid, the deep cycle battery, solar panel and power inverter can
237 be removed.

238 **4. Methods**

239 We completed all water vapor isotope analyses in the Stable Isotope Lab at the Institute
240 of Arctic and Alpine Research (INSTAAR SIL) at the University of Colorado Boulder between
241 October 2020 and August 2022. We used a Picarro L-2130i water isotope analyzer (Picarro, Inc.
242 Santa Clara, CA) to measure both water concentration and the oxygen and hydrogen isotope
243 ratios of the water vapor.
244

245 **4.1 QA/QC: Testing the SWISS under lab conditions**

246 Our highest order concern for the SWISS is that it remains leak-free, because leaks would
247 introduce the potential for fractionation or mixing of atmosphere that would alter the stable
248 isotope ratio of the water vapor in the flask. To mitigate leaks, we developed a three-part quality
249 assurance and quality control (QA/QC) procedure that must be completed for each new SWISS
250 prior to the first deployment. The first step detects any large, fast leaks using helium detection
251 methods; the second step detects medium scale leaks using dry air; and the third step detects
252 slow, small scale leaks using water vapor tests. Full procedural descriptions are available in the
253 supplemental material and the data processing code is available via GitHub.
254

255 ***4.1.1 Step 1: Use helium to detect large, fast leaks***

256 After initial assembly of the SWISS units, we looked for large leaks from the cracking of
257 inlet or outlet tubes on the glass flasks that occasionally occurred while tightening the Swagelok
258 fittings. To do this, we filled the flasks with helium and used a helium leak detector (Leak
259 Detector, Catalog #22655, Restek, Bellefonte, PA, USA). Another easy alternative to a helium
260 leak test is to complete a very short dry air test (methods described below) where the hold-time is
261 on the order of 12-24 hours.
262

263 ***4.1.2 Step 2: Use dry air to detect medium scale leaks***

264 The goal of this test was to catch any second order, medium-scale leaks associated with
265 either Valco valve fittings or Swagelok fittings that were under tightened.
266

267 *Step 2A: Fill flasks with dry air*

268 To start every experiment, we filled flasks with air that is filtered through Drierite (which
269 has a water vapor mole fraction of less than 500 ppm), at 2 L/min for 5 minutes. With a flask
270 volume of 650 ml, this means the volume of the flask is turned over 15 times.
271

272 *Step 2B: Hold period*

273 Flasks were then sealed and left to sit for seven days. This time period can be adjusted by
274 other users to fit their climate or needs.
275

276 *Step 2C: Measure water vapor mole fraction using dead-end pull sample introduction*

277 At the end of the seven-day period, we measured each flask using a dead-end pull sample
278 introduction method. For this sample introduction method, the inlet to the Valco valve was
279 sealed with a 1/4 inch Swagelok cap and there was no introduction of a carrier gas. As a result,
280 air was removed from the flask based on the flow rate of the Picarro analyzer (typically 27 - 31
281 ml/min). Flasks were measured for five minutes, which resulted in ~150 ml of air being removed
282 from the flasks. All components within the SWISS are capable of being fully evacuated. Water
283 vapor mole fractions determined by Picarro instruments are not standardized, so it is impossible

284 to know for sure the exact magnitude of water vapor mole fraction change between the input
285 analysis and the final value at the end of the dry air test. However, these instruments are
286 remarkably stable over weeks, and so the relative changes observed (e.g. increase or decrease of
287 mole fraction relative to the initial amount) are likely reliable, particularly for the larger
288 magnitude changes.

289 If a flask had a water vapor mole fraction of less than 500 ppm, it “passed” step 2 of
290 QA/QC. If a flask had a water vapor mole fraction greater than 500 ppm, it “failed” step 2 of
291 QA/QC, and we tightened both the Swagelok connections on the flasks as well as the fittings
292 between the stainless steel tubing and the Valco valve. We repeated dry air tests on any given
293 SWISS unit until the majority (typically at least 13/15) of the flasks had passed step 2 of QA/QC.
294

295 ***4.1.3 Step 3: Water vapor tests detect small scale leaks***

296 The purpose of this experiment was to mimic storage of water vapor at concentrations
297 similar to what we might expect in a soil, and for durations similar to those of our field
298 experiments. These experiments were meant to test whether flasks filled early in the sampling
299 sequence during field deployments leak by the time samples are returned to the lab for
300 measurement. For this experiment, we filled flasks with water vapor of known isotopic
301 composition and water vapor mole fraction, sealed the flasks for 14 days, and then measured the
302 water vapor mole fraction and isotope values of each flask. We performed 11 water vapor tests
303 that were done across three analytical sessions using six different SWISS units. Across these
304 three sessions, we measured 164 flasks both at the start of the 14-day experiment, and at the end.
305

306 *Step 3A: Flush flasks with dry air*

307 Prior to putting any water vapor into the flasks (either in the field or in the lab), we
308 completed a dry air fill (as described in QA/QC step 2A) that served to purge the flasks of any
309 prior water vapor that might exchange with the new sample.
310

311 *Step 3B: Fill flasks with water vapor and measure input isotope values*

312 To supply water vapor to the flasks, we used the vapor permeable probes that were
313 constructed identically to those deployed in the field. We immersed the probes up to the
314 connection between the vapor permeable and impermeable tubing in water, taking care to not
315 submerge the connection point and inadvertently allow liquid water to enter the inside of the
316 vapor permeable tubing. We flushed the flasks at a rate of 150 ml/min for 30 minutes, and
317 measured the $\delta^{18}\text{O}$ and $\delta^2\text{H}$ values and mole fraction of water vapor as each flask was filled. To
318 fill 15 flasks sequentially, the probes were submerged in water for approximately 7.5 hours.

319 Across three different sessions, we used three different waters that are tertiary standards
320 in the INSTAAR SIL to complete these experiments: a light water made from melting and
321 filtering Rocky Mountain snow ($\sim -25.5\text{‰}$ and -187.5‰ VSMOW, for $\delta^{18}\text{O}$ and $\delta^2\text{H}$,
322 respectively), an intermediate water that is deionized (DI) water from the University of Colorado
323 Boulder Campus ($\sim -16.2\text{‰}$ and -120.7‰ VSMOW for $\delta^{18}\text{O}$ and $\delta^2\text{H}$, respectively) and a heavy
324 water that is filtered water sourced from Florida, USA ($\sim -0.8\text{‰}$ and -2.8‰ VSMOW for $\delta^{18}\text{O}$
325 and $\delta^2\text{H}$, respectively). All tertiary lab standards are characterized relative to international
326 primary standards obtained from the International Atomic Energy Agency and are reported
327 relative to the VSMOW/SLAP standard isotope scale. To calculate the input value, we averaged
328 $\delta^{18}\text{O}$ and $\delta^2\text{H}$ values over the last three minutes of the filling period. We then stored the water

329 vapor in the flasks for 14 days. At the end of the 14-day storage period, we measured each flask
330 to evaluate if the $\delta^{18}\text{O}$ and $\delta^2\text{H}$ values had significantly changed over the storage period.

331
332 *Step 3C: Measure the water vapor isotope values*

333 To mitigate memory effects between flasks, we ran dry air via the flask bypass loop (port
334 one of every SWISS unit) for five minutes between each flask measurement. To verify that the
335 impermeable tubing between the SWISS and the Picarro instrument was sufficiently dried, we
336 waited until the water vapor mixing ratio being measured by the Picarro instrument was below
337 500 ppm for >30 seconds.

338 During this five-minute window, we used a heat gun to manually warm each flask. We
339 believe heating the flasks creates a more stable measurement by limiting water vapor bound to
340 the glass walls of the flask and by helping to homogenize the water vapor within the flask. While
341 we did not strictly control or regulate the temperature of the flasks, they were all warm to the
342 touch.

343 Once we warmed the flask and dried the impermeable tubing, water vapor was introduced
344 to the CRDS using one of two methods: 1) the dead-end pull sample introduction method
345 described above, or 2) a *dry air carrier gas sample introduction* method. During the dry air
346 carrier gas sample introduction method, dry air is continuously flowing through the flask at a rate
347 of 27-31 ml/min for the entire 12-minute measurement period. To reach a water vapor mole
348 fraction of approximately 25,000 ppm (the optimal humidity range for the Picarro L2130-*i*), we
349 diluted the water vapor with dry air at a rate of 10 ml/min. Without dilution, the concentration
350 out of the flasks is as high as 35,000 - 40,000 ppm, which leads to linearity effects on a Picarro
351 L2130-*i* that can be challenging to correct for. The dead-end pull method is preferable when the
352 water vapor mole fraction inside the flask is low (<17,000 ppm), because there is no additional
353 introduction of dry air. The introduction of dry air decreases the water vapor mole fraction
354 throughout the measurement, and in fairly dry flasks, using the dry air carrier gas method can
355 lower the water vapor mole fraction to below 10,000 ppm. Below 10,000 ppm, there are large
356 linearity isotope effects associated with the measurement on a Picarro L2130-*i*, and the isotope
357 values are challenging to correct into a known reference frame, just as with high water vapor
358 mole fractions. The major downside of the dead-end pull method is that condensation is more
359 likely to form in the stainless-steel tubing that connects the flasks to the Valco valve, as well as
360 the Valco valve itself, compared to the dry air carrier gas method. The dry air carrier gas method
361 prevents condensation from forming in the Valco valve and tubing, and prevents fractionation
362 that may occur because of changing pressure within the flask. It is possible that during a dead-
363 end pull on the flask, heavier isotopes may remain attached to the walls of the flask, coming off
364 later as the pressure drops. For these reasons, the dry air carrier gas sample introduction method
365 is our preferred method for sample introduction in most cases.

366 For each flask, we looked at the stability of the isotope values as well as either a stable
367 water vapor mole fraction if the dead end pull method was being used or a steady, linear decrease
368 in water vapor mole fraction if the dry air carrier gas method was being used. For approximately
369 90% of the flasks we found that after excluding the first three minutes of measurement of each
370 flask, the subsequent three minutes were the most stable. For the remaining ~10% of the flasks,
371 using a time window that started either ~30 seconds earlier or ~30 seconds later to create an
372 average isotope value offered a more stable isotope signal with smaller instrumental
373 uncertainties. Any flask that required specialized treatment during the data reduction process was
374 flagged during measurement.

375

376 *Step 3D: Data correction*

377 During these experiments, we monitored instrument performance (e.g. drift) in two ways.
378 First, to run standards identically to how samples were collected, we introduced tertiary
379 standards, described above, using vapor probes. The water vapor produced by the vapor
380 permeable probes was flushed through the SWISS unit via the flask bypass loop and diluted with
381 a 10 ml/min dry air flow to reach a water vapor mole fraction of approximately 25,000 ppm
382 before entering the Picarro instrument. Second, we introduced a suite of four secondary
383 standards that have been calibrated against primary standards, and reported against
384 VSMOW/SLAP via a flash evaporator system described in detail by Rozmiarek and others
385 (2021). This flash evaporator system can be used to adjust the water vapor mole fraction to
386 create linearity corrections at high and low water vapor mole fractions. After correcting data into
387 a common reference frame, we calculated the difference between the input isotope values and the
388 ending isotope values.

389 The results of these tests were used to carefully document flasks that do not perform well,
390 and any idiosyncrasies of SWISS units. That way, during field deployment suspicious flasks
391 could be easily identified and investigated.

392

393 **4.2 Field suitability experiments:**

394 ***4.2.1 Field suitability experiment #1: Long term field dry air test***

395 As a complement to the QA/QC we did under lab conditions, we also completed long
396 term dry air tests at our field sites. We had three goals associated with these experiments. The
397 first was to test whether, even under field conditions, where daily temperature and relative
398 humidity fluctuations are different than in a lab setting, the flasks were still resistant to
399 atmospheric intrusion. Second, we used these tests to evaluate whether the flasks that were
400 flushed with soil water vapor near the end of a sampling sequence took on atmosphere prior to
401 sampling. Lastly, we chose these time intervals because they bracket the typical length of a
402 deployment, which helped us determine how quickly flasks should be measured after bringing a
403 SWISS back to the lab.

404 Like all field deployments, we started with a dry air fill, and then one SWISS unit was
405 deployed to each of our three field sites. No soil water was collected during these deployments.
406 The duration between filling the flasks with dry air to measuring the flasks was between 34 - 52
407 days. The 34 and 52 day tests were done during June 2022 and August 2021, respectively, and
408 therefore tests the SWISS under warm summertime conditions. The 43 day test was done in
409 October 2021, which included nights where air temperatures fell below 0°C. The only barrier
410 between air and the SWISS in its deployment hole was a plywood board, and so this deployment
411 tested the suitability of the SWISS to maintain integrity under freezing conditions.

412

413 ***4.2.2. Field suitability experiment #2: Mock field tests***

414 To test whether the automation code and sampling scheme we developed worked as
415 expected on short, observable timescales, we set up an experiment to simulate field deployment
416 of one SWISS unit (Meringue) near the University of Colorado Boulder. This test applied the
417 automation components and remote power setup described in the materials section. During this
418 field-simulation experiment, our goal was to collect three discrete samples each sampling period,
419 to simulate the collection of water vapor from three soil depths. An important goal of this test

420 was to test whether the sampling scheme introduced any memory effects between samples. We
421 followed the sampling protocol described in figure 2 and table 1.

422 The day before the experiment began, all flasks were flushed with dry air as described in section
423 4.1.2. Over the course of 25 hours, all 15 flasks were filled with three different vapors according
424 to a set schedule as would be done in the field. Two of the vapors were created by immersing the
425 water vapor permeable probes in the light water and intermediate water as described in section
426 4.1.3. The third was water vapor from the ambient atmosphere. All three vapors were sampled
427 using vapor permeable probes constructed identically to those deployed in the field. For this
428 experiment, we filled three flasks per cycle with each one of the waters (e.g. Flask 2 = light,
429 Flask 3 = intermediate, Flask 4 = atmosphere). The choice to sample atmosphere alongside two
430 waters reflects our second goal of this test, which was to demonstrate that sampled water vapor
431 isotope values do not drift towards atmospheric values (Magh et al., 2022).

432 Following the sampling schedule, we stored the SWISS unit in a simulated field setting
433 for seven days. At the end of the seven days, we measured the flasks. For flasks that had a high
434 water vapor mole fraction (i.e. light and intermediate water vapor samples) we used the dry air
435 carrier gas sample introduction method. For flasks that had a low water vapor mole fraction (i.e.
436 atmosphere, ~15,000 ppm) we used the dead end pull sample introduction method.

437 To create average values for each flask, we followed the same averaging protocol
438 described in section 4.1.3. We used equations 2A and 2B from Rothfuss et al., (2013) to convert
439 from water vapor to liquid values. Then, using secondary and tertiary standards, data were
440 corrected into the VSMOW/SLAP isotope scale. Finally, the SWISS unit offset correction
441 (detailed below in section 6.1.2) was applied.

442 443 **4.3 Example Field Deployment: One month period**

444 We deployed one SWISS unit each to the three field sites described in summer 2022.
445 Before deployment, all SWISS units were flushed with dry air following the protocol outlined in
446 section 4.1.2. Flasks were flushed with dry air one to three days prior to field deployment. At
447 each site, we sampled at three depths (25 cm, 50 cm, and 75cm) on each sampling day, following
448 the protocol described in figure 2 and table 1. We sampled soil water from all three depths every
449 five days (protocol length = 25 days total). At Oglala National Grassland, samples were taken
450 every five days from 2022-06-25 to 2022-07-14. At the Briggsdale, CO site samples were taken
451 every five days between 2022-07-17 and 2022-08-06. At the Seibert, CO site, samples were
452 collected every five days between 2022-06-19 and 2022-07-04. At the end of a 28-day period,
453 the SWISS units were returned to the lab, and measured. SWISS units were measured within five
454 days of returning from the field. The maximum number of days a flask held sample water vapor
455 during these deployments was 32 days. The measurement protocol and data averaging protocol
456 follows the procedures described in section 4.1.3. The data correction scheme follows as in the
457 section 4.2.2.

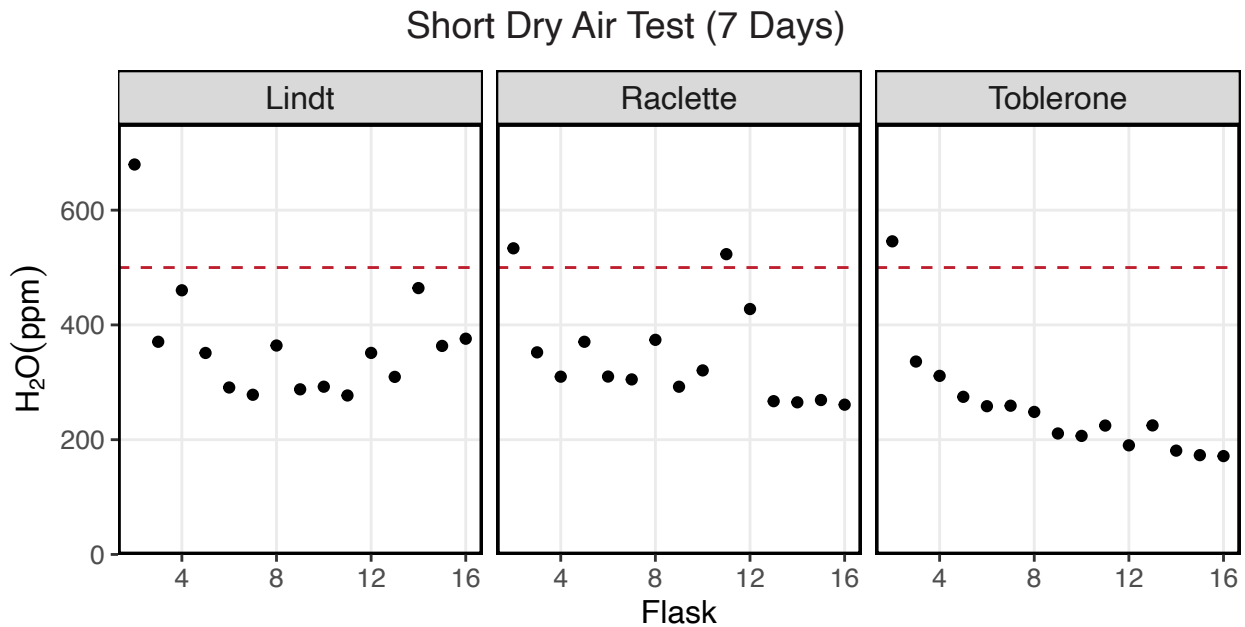
458 **5 Results**

459 **5.1 QA/QC Results**

460 **5.1.1 Dry air test**

461 Figure 3 shows the results of a seven-day dry air test for three SWISS units (marked by
462 the unit name) (SI Table 3). For all three SWISS units, at least 13/15 of the flasks maintained a
463 water vapor mole fraction value of less than 500 ppm over the seven-day period. In two of the

464 three SWISS units (Lindt and Raclette), the water vapor mole fraction for flasks was randomly
 465 distributed around approximately 350 ppm. In Toblerone there was a systematic decrease in
 466 water vapor mole fraction from flask two through flask 16, matching the order in which the
 467 flasks were filled with dry air initially. In all three SWISS units, flask two had the highest water
 468 vapor mole fraction of all the flasks. Supplemental figure 2 shows the results of successive dry
 469 air tests on the SWISS unit Toblerone where Swagelok fittings were tightened between tests.
 470 Between the two tests, there was a significant decrease in measured water vapor mole fraction
 471 for many flasks, but particularly for flasks 10 and 11 as a result of tightening the fittings.



472
 473 **Figure 3. Results of a dry air test from three different SWISS units named: Lindt, Raclette and Toblerone. The majority**
 474 **of the flasks maintain a water vapor mixing ratio of less than 500 ppm.**
 475

476 **5.1.2. Water vapor test**

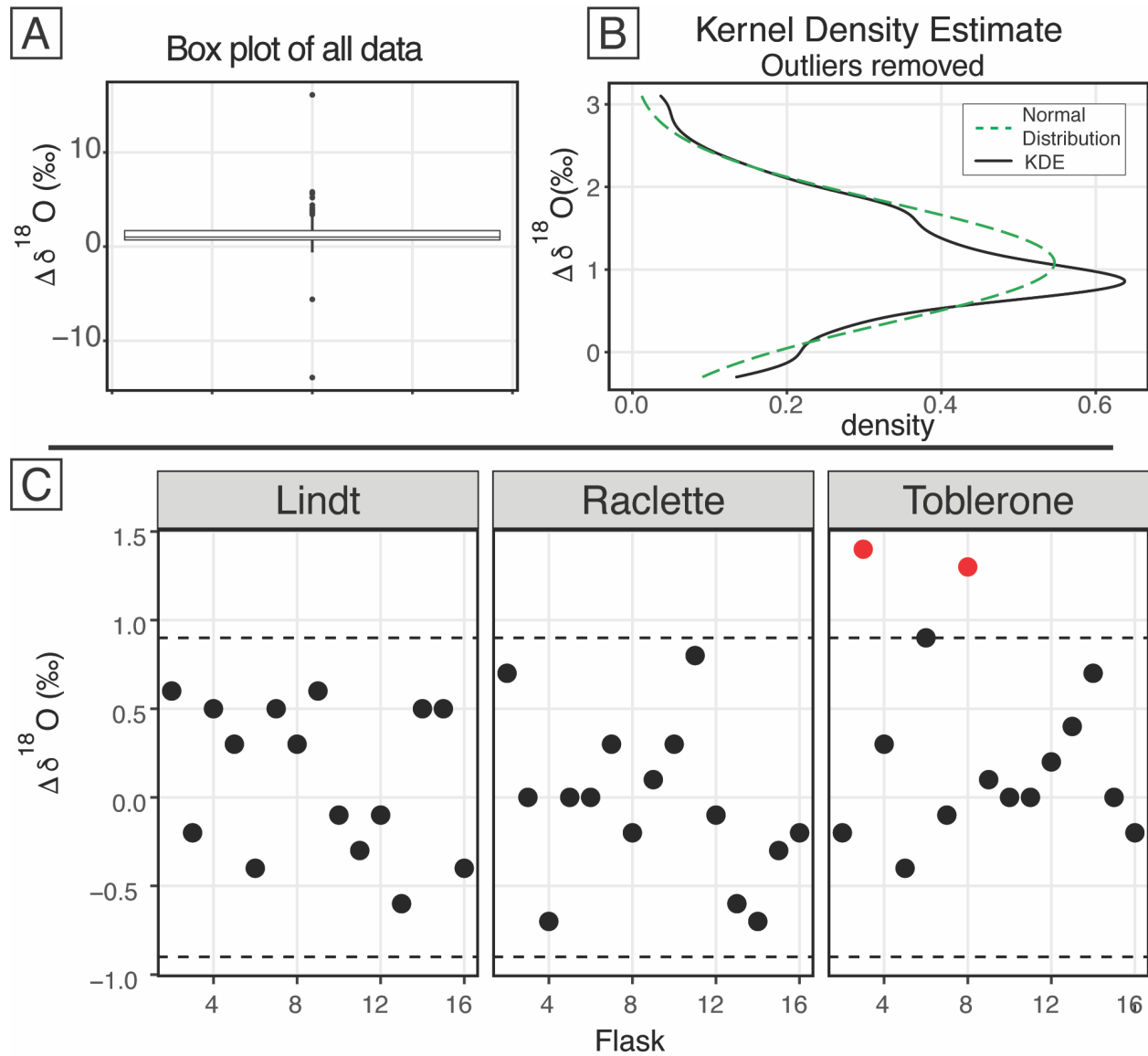
477 Figure 4 shows the $\delta^{18}\text{O}$ results of 11 water vapor tests performed using six different
 478 SWISS units. Ideally, we expect a normal distribution centered about 0 within the uncertainty
 479 limits of the water vapor probes (Oerter et al., 2016). For $\delta^{18}\text{O}$, the mean difference between the
 480 start and end values for the flasks is 1.1‰ with a standard deviation of 0.72‰ (outliers
 481 removed). There is a consistent positive offset, with a few clear outliers (Fig. 4A). We do not
 482 observe a consistent difference between water vapor sample introduction methods (Supplemental
 483 Fig. 3). After removing outliers ($< Q1 - 1.5 * IQR$ or $> Q3 + 1.5 * IQR$, $n = 15$) from the dataset,
 484 we compared the kernel density estimate shape to a normal distribution calculated from the mean
 485 and standard deviation of the dataset to assess dataset normality (Fig. 4B). A normal distribution
 486 slightly overestimates the center of the data, but captures the overall shape fairly well. Therefore,
 487 we used the median offset (1.0‰) to correct our water vapor isotope values, and used the
 488 interquartile range of the dataset (outliers removed) to estimate uncertainty of the SWISS as \pm
 489 0.9‰. In figure 5C, for simplicity, we just present the results from 45 flasks (three SWISS units),
 490 with the 1.0‰ offset correction applied. After correction, data are randomly distributed about 0,
 491 and are within the uncertainty range of $\pm 0.9‰$ (Supp. Table 4).

492 Figure 5 shows the $\delta^2\text{H}$ results of 11 water vapor tests. For $\delta^2\text{H}$, the mean difference
 493 between the start and end values is 2.63‰ with a standard deviation of 2.85‰ (outliers

494 removed). Similar to $\delta^{18}\text{O}$, we expected a normal distribution of differences centered around 0.
495 As with $\delta^{18}\text{O}$, there was a consistent positive offset with some outliers (i.e., $< Q1 - 1.5 \cdot \text{IQR}$ or $>$
496 $Q3 + 1.5 \cdot \text{IQR}$) (Fig. 5A). After removing outliers ($n = 26$) from the dataset, we compared the
497 kernel density estimate to a normal distribution calculated from the mean and standard deviation
498 of the dataset to assess dataset normality (Fig. 5B). As with $\delta^{18}\text{O}$, the center of the dataset is
499 overestimated by the mean, but the overall peak shape is roughly captured. We therefore use the
500 median value of 2.3‰ as an offset correction and estimate uncertainty at $\pm 3.7\%$ for $\delta^2\text{H}$ from the
501 interquartile range. In figure 5C, we present the results from 45 flasks (three SWISS units), with
502 the 2.3‰ offset correction applied. Data are randomly distributed about 0 and are within the
503 uncertainty range of $\pm 3.7\%$ (Supplemental Table 4).

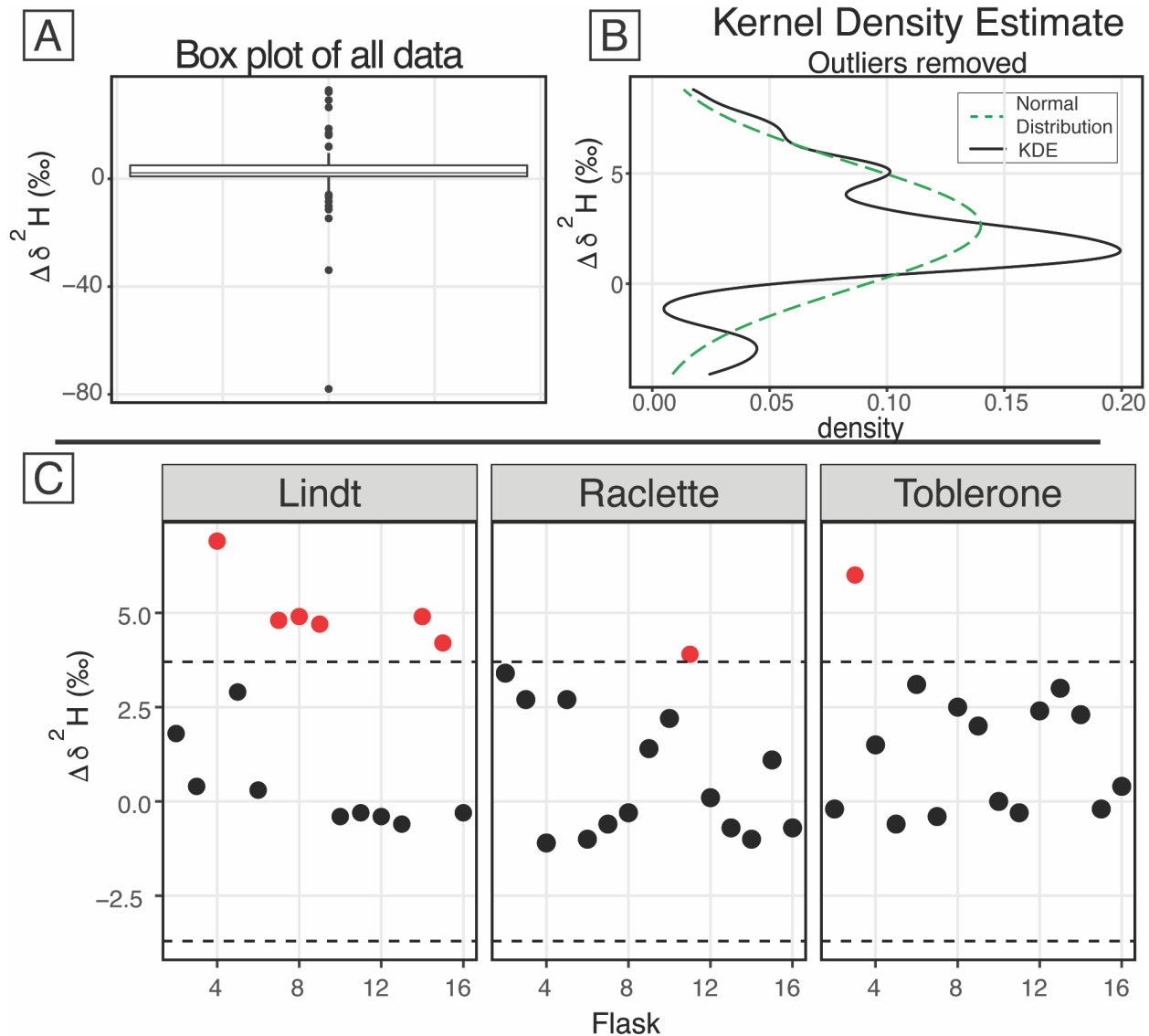
504 When we compared the results in figures 4C and 5C, we found that flasks that performed
505 adequately for $\delta^{18}\text{O}$ did not always perform adequately for $\delta^2\text{H}$. The results from the SWISS unit
506 Lindt display this behavior particularly well. Less commonly, some flasks that were within
507 uncertainty of the system for $\delta^2\text{H}$ were not within uncertainty of the system for $\delta^{18}\text{O}$, like flask
508 eight in the SWISS unit Toblerone (Figs. 4C, 5C). In a dual isotope plot, there is a strong
509 positive correlation between $\delta^2\text{H}$ and $\delta^{18}\text{O}$ with a slope of 3.14 and an R^2 value of 0.62
510 (Supplemental Fig. 4).

511



513
514
515
516
517
518
519
520
521
522
523
524
525

Figure 4. $\delta^{18}\text{O}$ results of the water vapor tests. A) Boxplot of the difference between the starting $\delta^{18}\text{O}$ value and the final $\delta^{18}\text{O}$ value of all 164 flasks. B) After removing the outliers from the dataset, the kernel density estimate (black line) and the normal distribution calculated from the dataset (dashed green) are shown. C) After applying the offset correction of 1.0‰, the difference between the starting $\delta^{18}\text{O}$ value and the final $\delta^{18}\text{O}$ value for three boxes from the August 2022 session are shown. An uncertainty of $\pm 0.9\text{‰}$ is marked with a dashed line, and data points that fall outside that uncertainty are colored red.



526
 527
 528 **Figure 5.** $\delta^2\text{H}$ results of the water vapor tests A) Boxplot of the difference between the starting $\delta^2\text{H}$ value and the final $\delta^2\text{H}$ value
 529 of all 164 flasks. B) After removing the outliers from the dataset, the kernel density estimate (black line) and the normal
 530 distribution calculated from the dataset (dashed green) are shown. C) The difference between the starting $\delta^2\text{H}$ value and the final
 531 $\delta^2\text{H}$ value for three boxes from the August 2022 session are shown after applying the offset correction of 2.3‰. An uncertainty of
 532 $\pm 3.7\%$ is marked with a dashed line, and data points that fall outside that uncertainty are colored red.
 533

534 **5.2 Field suitability test results**

535 **5.2.1 Dry air test**

536 Figure 6A shows the result of placing three different SWISS units that were flushed with
537 dry air out into the field for 34 - 52 days (SI Table 3). This timescale (four - six weeks) is similar
538 to most field deployments. At the timescale of 34 - 43 days, 13 of the 15 flasks typically
539 maintained a water vapor mole fraction of less than 1000 ppm. Over the 52 days, seven flasks
540 maintained a water vapor mole fraction less than 1000 ppm and the remaining eight had a water
541 vapor mole fraction between 1000 - 2500 ppm.

542

543 **5.2.2 Automation test**

544 Figure 6B shows the results of using the automation code to collect and store water vapor
545 of known composition for seven days (Table 2). In both plots, the known values of the water are
546 shown as a long-dash line. Uncertainty on those measurements is estimated at $\pm 0.5\text{‰}$ and $\pm 2.4\text{‰}$
547 for $\delta^{18}\text{O}$ and $\delta^2\text{H}$, respectively (Oerter et al., 2016), shown as the dotted lines. We estimated the
548 isotope value of the atmosphere at the time of sampling with water vapor mole fraction, $\delta^{18}\text{O}$,
549 and $\delta^2\text{H}$ data from the CRDS in the lab. The isotope value, that was corrected as described in
550 section 4.2.2, of each flask is shown, with uncertainty associated with the SWISS units estimated
551 at $\pm 0.9\text{‰}$ and $\pm 3.7\text{‰}$ for $\delta^{18}\text{O}$ and $\delta^2\text{H}$, respectively.

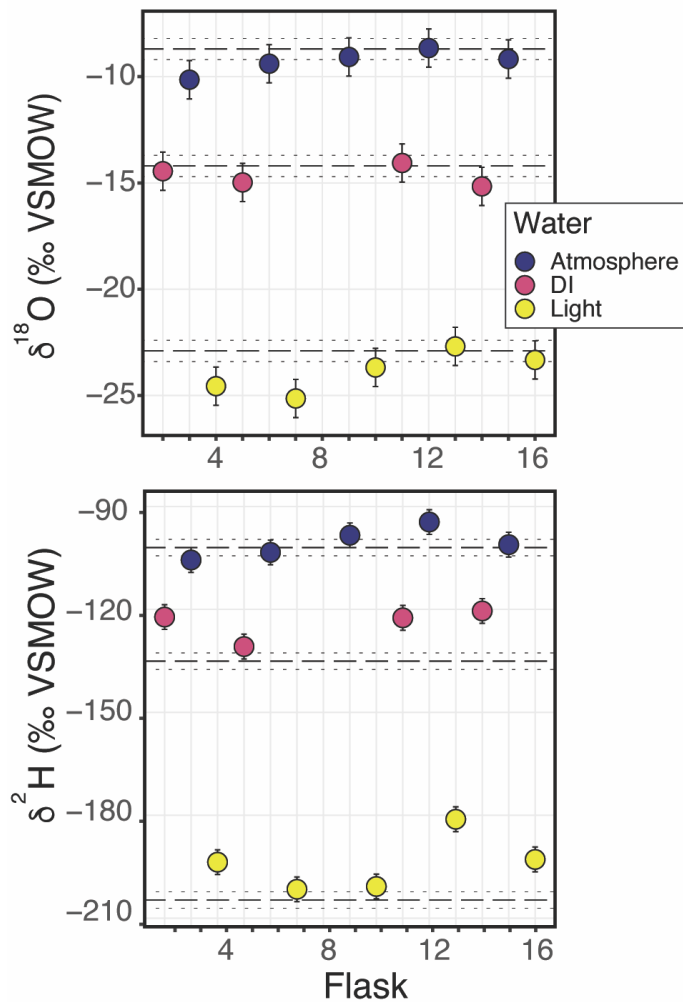
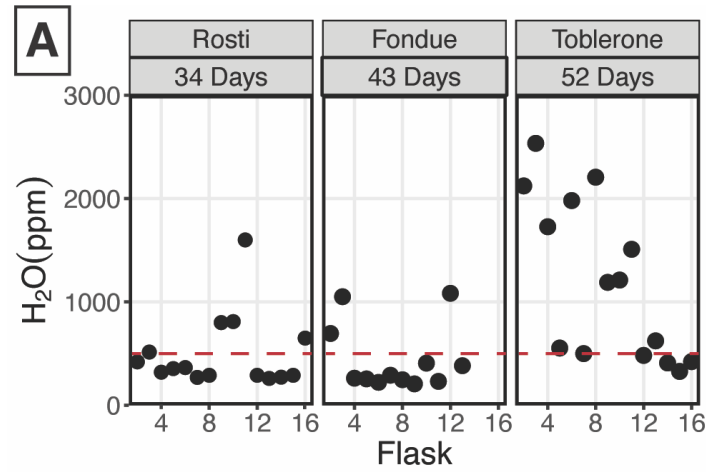
552 Seven of the nine flasks filled with flash-evaporated water vapor overlap within
553 uncertainty of the known $\delta^{18}\text{O}$ value for those standards (top plot, Fig. 6B), and four of the five
554 flasks filled with atmospheric vapor overlap within uncertainty of our estimated $\delta^{18}\text{O}$ value.
555 Flasks that fall outside of the bounds of uncertainty have lower $\delta^{18}\text{O}$ values than the expected
556 value. For $\delta^2\text{H}$, (bottom plot, Fig. 6B) only three of the nine flasks filled with flash-evaporated
557 water vapor overlap within uncertainty of the known value of those standards, while four of the
558 five flasks filled with atmospheric vapor overlap within uncertainty of the estimated $\delta^2\text{H}$ value.
559 Flasks that fall outside of the bounds of uncertainty have higher $\delta^2\text{H}$ values than the expected
560 value.

561

562 **Table 2.** Results of the Automation test

SWISS	Flask	water	δ¹⁸O (‰)	δ²H (‰)
Meringue	2	DI	-14.4	-122.2
Meringue	3	Atmosphere	-10.1	-105.6
Meringue	4	Light	-24.6	-193.7
Meringue	5	DI	-15.0	-130.8
Meringue	6	Atmosphere	-9.4	-103.4
Meringue	7	Light	-25.1	-201.5
Meringue	8	DI	-17.3	-140.5
Meringue	9	Atmosphere	-9.1	-98.4
Meringue	10	Light	-23.7	-200.7
Meringue	11	DI	-14.1	-122.5
Meringue	12	Atmosphere	-8.7	-94.5
Meringue	13	Light	-22.7	-181.2
Meringue	14	DI	-15.2	-120.5
Meringue	15	Atmosphere	-9.2	-101.1
Meringue	16	Light	-23.3	-192.9

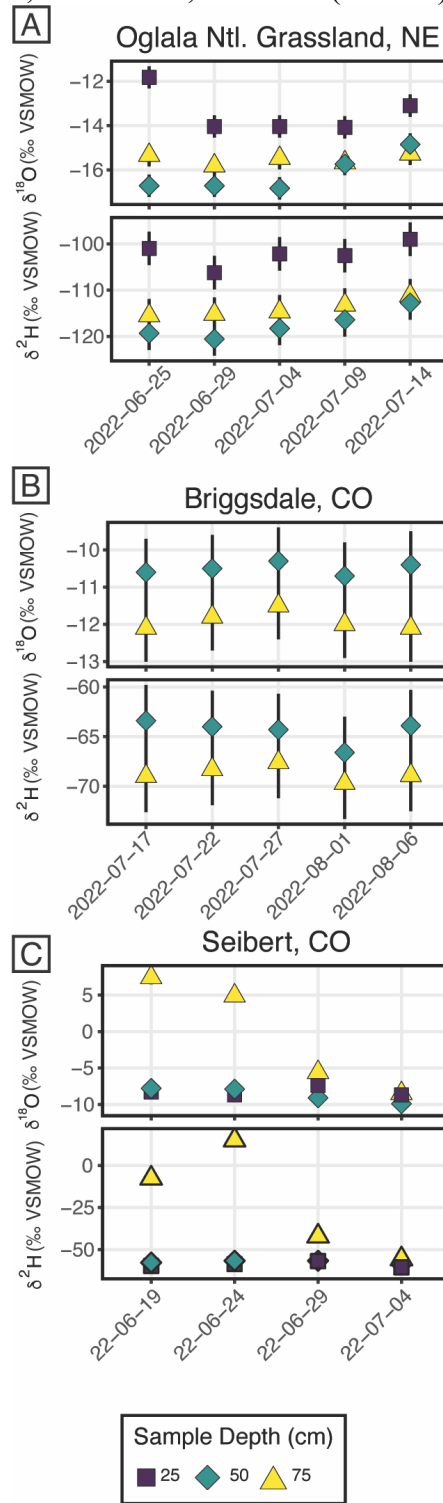
563



564
 565 **Figure 6.** A) Results from three different field-based long dry air tests. B) Results from the automation
 566 field suitability tests using the SWISS unit named Meringue. Flasks that sampled atmosphere are shown
 567 in blue, flasks that sampled deionized water (DI) are shown in pink, and flasks that sampled the light
 568 water are shown in yellow. The top plot shows the δ¹⁸O results, and the bottom plot shows the δ²H results.
 569

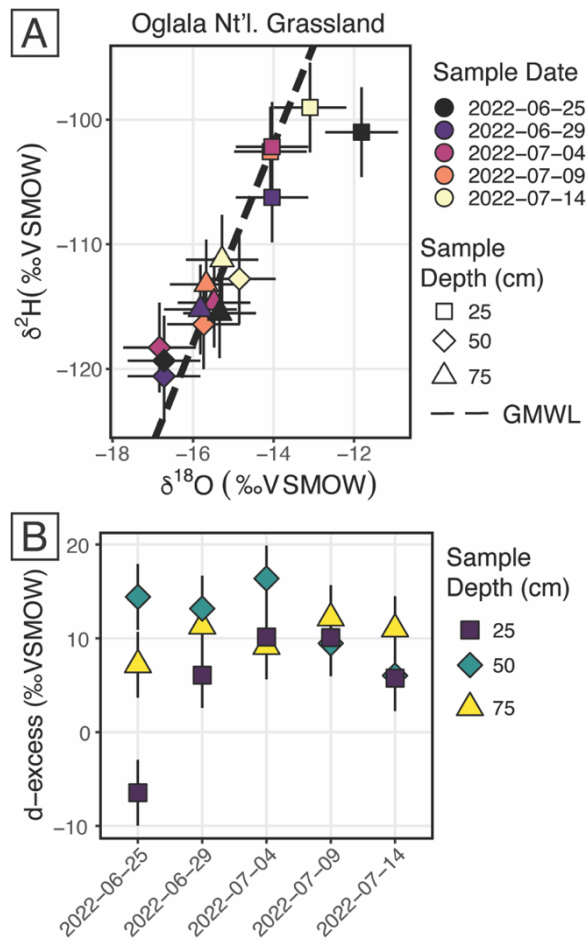
570 **5.3 Example Field deployment results**

571 Figure 7 shows the results from three field deployments in Oglala National Grassland,
 572 Nebraska; Briggsdale, Colorado; and Seibert, Colorado (Table 3).



573 **Figure 7.** Results from all three field deployments to A) Oglala National Grassland, NE, B) Briggsdale,
 574 CO and C) Seibert, CO. Note, the y-axis scale for all three plots is different.
 575

576 There are 15 samples from Oglala National Grassland (Fig. 7A, Table 3); five from 25
 577 cm depth, five from 50 cm depth and five from 75 cm depth. Four of the five samples from 25
 578 cm overlap within uncertainty in $\delta^{18}\text{O}$ value, and all five samples overlap with uncertainty in $\delta^2\text{H}$
 579 value. There is a significant decrease in the $\delta^{18}\text{O}$ value at 25 cm between 2022-06-25 and 2022-
 580 06-29. There is no similar shift in $\delta^2\text{H}$ value over the same time period. The first three samples
 581 from 50 cm overlap in both $\delta^{18}\text{O}$ and $\delta^2\text{H}$ values, then the final two samples shift to higher
 582 isotope values. Similar to the samples from 50 cm, there is a trend towards higher $\delta^2\text{H}$ values for
 583 the last three samples. All five samples from 75 cm overlap in $\delta^{18}\text{O}$ and $\delta^2\text{H}$ values. On a dual
 584 isotope plot, data from 50 cm and 75 cm cluster together at lower values, while the $\delta^{18}\text{O}$ and $\delta^2\text{H}$
 585 values from 25 cm are higher (Figs. 7A, 8A). All of the data overlap within uncertainty with the
 586 global meteoric water line, except for the 25 cm depth sample from 2022-06-25 (Fig. 8A). The
 587 calculated d-excess values are all within uncertainty of 10‰ ($\pm 2.6\%$) and of each other between
 588 2022-06-29 and 2022-07-14 (Fig 8B), except for the 25 cm depth sample from 2022-06-25,
 589 which has a d-excess value of -6.6‰, typically consistent with evaporative enrichment of soil
 590 water at that depth and time.
 591



592
 593 **Figure 8.** Results from the Oglala National Grassland, NE field site. A) $\delta^2\text{H}$ vs. $\delta^{18}\text{O}$, where the dashed
 594 line is the global meteoric water line. The shapes for the different depths sampled matches figure 7, and
 595 the color of the points is the date on which the soil water was sampled B) A plot of d-excess. Note, both
 596 the color and shape match figure 7.

597 There are 10 samples from Briggsdale, CO (Fig. 7B, Table 3); five samples each from
598 vapor probes buried at 50 cm and 75 cm depth. Data from 25 cm at Briggsdale, CO were
599 excluded because the water vapor mole fractions from all of the flasks were extremely low
600 (<13,000 ppm). We excluded these data because these samples are associated with a very dry
601 soil (VWC < 0.05), and it is not clear how much sampling gas (N₂) is injected into the soil using
602 the vapor permeable tubing under very dry conditions (Quade et al., 2019), and therefore how
603 representative these isotope data are of soil water. Moreover, below 13,000 ppm there are large
604 linearity effects on a Picarro L2130-*i*, and it is challenging to correct those data if they were
605 measured using the dry-air carrier sample introduction method. While all samples overlap within
606 uncertainty for both $\delta^{18}\text{O}$ and $\delta^2\text{H}$ values, the absolute values of samples from 50 cm are
607 consistently offset to higher values for both $\delta^{18}\text{O}$ and $\delta^2\text{H}$ as compared to samples from 75 cm.

608 There are 12 samples from Seibert, CO (Fig. 7C, Table 3); four from each sampling depth
609 (25, 50 and 75 cm). At 25 cm depth, $\delta^{18}\text{O}$ values of three of the four samples overlap within
610 uncertainty, while the 25 cm sample from 2022-06-29 has a higher $\delta^{18}\text{O}$ value than the other
611 three samples. At 25 cm depth, $\delta^2\text{H}$ values overlap within uncertainty for all four samples. At 50
612 cm depth, there is a steady decrease in $\delta^{18}\text{O}$ value over the sampling period, while $\delta^2\text{H}$ values for
613 all four samples remain steady and overlap within uncertainty. At 75 cm depth, samples have a
614 very large range of $\delta^{18}\text{O}$ values between -8.5‰ and 7.4‰, and $\delta^2\text{H}$ values range between -
615 55.7‰ and 15.1‰.

616 **Table 3.** Results from the three field deployments of SWISS.

Site	Date	Sample Depth (cm)	Flask	T (°C)	$\delta^{18}\text{O}$ (‰)	$\delta^{18}\text{O}$ (‰) Analytical Error	$\delta^2\text{H}$ (‰)	$\delta^2\text{H}$ (‰) Analytical Error
Briggsdale	2022-07-17	50	3	25.1	-10.8	0.2	-65.6	0.6
Briggsdale	2022-07-17	75	4	23	-12.1	0.2	-69	0.7
Briggsdale	2022-07-22	50	6	25.9	-10.7	0.3	-67.1	0.7
Briggsdale	2022-07-22	75	7	23.6	-11.9	0.2	-69	0.6
Briggsdale	2022-07-27	50	9	24.3	-10.4	0.3	-65.6	0.6
Briggsdale	2022-07-27	75	10	23	-11.5	0.2	-67.6	0.7
Briggsdale	2022-08-01	50	12	23.4	-10.7	0.2	-67	0.7
Briggsdale	2022-08-01	75	13	22.4	-12.0	0.2	-69.1	0.7
Briggsdale	2022-08-06	50	15	24	-10.5	0.2	-65	0.6
Briggsdale	2022-08-06	75	16	22.9	-12.1	0.2	-68.8	0.7
Seibert	2022-06-19	25	2	24.2	-8.3	0.2	-59.8	0.6
Seibert	2022-06-19	50	3	22	-7.8	0.2	-57.8	0.6
Seibert	2022-06-19	75	4	19.4	7.4	0.2	-7.6	0.7
Seibert	2022-06-24	25	5	24	-8.7	0.2	-58.7	0.7
Seibert	2022-06-24	50	6	22.2	-7.9	0.2	-56.7	0.7
Seibert	2022-06-24	75	7	20.5	4.9	0.2	15.1	0.6
Seibert	2022-06-29	25	8	23.2	-7.4	0.2	-56.9	0.6
Seibert	2022-06-29	50	9	21.8	-9.1	0.2	-56.7	0.7
Seibert	2022-06-29	75	10	21	-5.6	0.2	-42.1	0.6
Seibert	2022-07-04	25	11	25	-8.7	0.2	-60.6	0.7
Seibert	2022-07-04	50	12	23.3	-9.9	0.2	-58.8	0.6
Seibert	2022-07-04	75	13	21.5	-8.5	0.2	-55.7	0.7
Oglala Ntl. Grassland	2022-06-25	25	2	23.0	-11.8	0.2	-101	0.7
Oglala Ntl. Grassland	2022-06-25	50	3	22.8	-16.7	0.2	-119.3	0.7
Oglala Ntl. Grassland	2022-06-25	75	4	21.5	-15.3	0.2	-115.5	0.8
Oglala Ntl. Grassland	2022-06-29	25	5	25.0	-14	0.2	-106.2	0.7
Oglala Ntl. Grassland	2022-06-29	50	6	22.8	-16.7	0.2	-120.6	0.7
Oglala Ntl. Grassland	2022-06-29	75	7	21.3	-15.8	0.2	-115.2	0.7
Oglala Ntl. Grassland	2022-07-04	25	8	25.0	-14	0.2	-102.2	0.7
Oglala Ntl. Grassland	2022-07-04	50	9	23.0	-16.8	0.2	-118.3	0.6
Oglala Ntl. Grassland	2022-07-04	75	10	22.0	-15.5	0.2	-114.7	0.6
Oglala Ntl. Grassland	2022-07-09	25	11	23.0	-14.1	0.2	-102.6	0.6
Oglala Ntl. Grassland	2022-07-09	50	12	22.8	-15.7	0.2	-116.4	0.7
Oglala Ntl. Grassland	2022-07-09	75	13	22.0	-15.7	0.2	-113.2	0.6
Oglala Ntl. Grassland	2022-07-14	25	14	23.0	-13.1	0.2	-99	0.6
Oglala Ntl. Grassland	2022-07-14	50	15	22.8	-14.9	0.3	-112.8	0.7
Oglala Ntl. Grassland	2022-07-14	75	16	22.0	-15.3	0.2	-111.2	0.7

617
618

619 6. Discussion

620 6.1 QA/QC and field suitability tests

621 6.1.1 Dry Air tests

622 In Colorado, where these tests were completed, the ambient atmosphere during the
623 summertime typically sits at a water vapor mole fraction between 10,000 - 20,000 ppm, and in
624 winter the water vapor mole fraction can drop as low as 4000 ppm. If the flasks had been slowly
625 equilibrating with the atmosphere, the flasks would have drifted to much higher water vapor
626 molar fractions. If the flasks did not drift towards higher water vapor mole fractions, we felt
627 confident that the flasks were resistant to atmospheric intrusion after they have been flushed with
628 dry air. We chose a timescale of seven days for the dry air tests because we found that in a low-
629 humidity environment, seven days was enough time to meaningfully observe leaks, while being
630 short enough to work through the QA/QC process efficiently. For example, results of two
631 sequential dry air tests on the SWISS unit Toblerone (supplemental Fig. 2), show that it is
632 possible to drastically reduce leaks that allow ambient water vapor from intruding into the flasks
633 by tightening and/or replacing problematic fittings (both those attached to the glass flasks and
634 those on the Valco valve) and in some rare cases the glass flask itself. During the final seven-day
635 dry air tests, most flasks maintained a water vapor mole fraction less than 400 ppm, and all flasks
636 maintained a water vapor mole fraction of less than 700 ppm (Fig. 3).

637 Across all of the SWISS units, there is a bias towards a higher water vapor mole fraction
638 for the first flask that is measured (port one on every valve is the flask bypass loop, so the first
639 flask is flask two), which suggests a methodological source of higher water vapor concentration
640 rather than Swagelok fitting tightness problems. There are two potential sources for this issue.
641 First, it is possible that not all of the atmospheric water vapor was flushed from the line that
642 connects to the CRDS prior to the start of the measurements, but by the time the second flask is
643 measured, the lines between the SWISS and CRDS have been sufficiently flushed, creating bias
644 in the first flask measured. This hypothesis could be tested by flushing all of the gas lines with
645 dry air to progressively lower water vapor mixing ratios prior to measuring any flasks, to see
646 what minimum ratio is required to eliminate this bias. Lab protocols could then be adjusted to
647 flush all gas lines to this level. Similarly, it is possible that during the filling phase, not all of the
648 atmospheric vapor has been flushed out of the Drierite system before starting the fill process.
649 This hypothesis is supported by the systematic decrease in water vapor mole fraction across
650 flasks in the Toblerone unit (Fig. 3, right panel). As a result of these biases, we now flush the
651 Drierite for at minimum 30 minutes prior to the start of the experiment.

652 In addition to testing the leakiness, the dry air test also provided a useful baseline from
653 which to test building materials. For example, in supplemental figure 5, we show the results of
654 sequential seven day and 27-day dry air tests where we replaced stainless steel tubing and fittings
655 with PTFE Swagelok fittings with 1/8 inch PTFE tubing. We thought that PTFE fittings would
656 be advantageous because they are much easier to install and are significantly lighter, and would
657 therefore be helpful when there are weight constraints. However, based on the very limited
658 testing we did, PTFE fittings and tubing *may be* sufficient to store water for up to a single week,
659 but on longer timescales (e.g. 27 days) we observed greater exchange and leaking than with the
660 stainless steel fittings. We encourage any future user using this modification to rigorously test
661 these fittings on a timescale appropriate for their application.

662

663 **6.1.2 Water vapor tests**

664 Our initial goal with the water vapor tests was to test whether the measured water vapor
665 isotope values at the end of the two-week holding period were normally distributed about 0
666 within the uncertainty limits of the water vapor probes (Oerter et al., 2016). This was a
667 reasonable goal given the similarities in probe set-up and the plumbing design between the
668 SWISS and the IsoWagon system (Oerter et al., 2016). But, the most salient result of the water
669 vapor tests is that there is a consistent positive offset between the input isotope values and the
670 isotope values measured at the end of the two-week experiments (Figs 4B, 5B). The positive
671 offset in both $\delta^{18}\text{O}$ and $\delta^2\text{H}$ values is consistent across 11 different tests, using six different
672 SWISS and three different input water isotope values. If there was alteration of original values
673 due to leaky flasks, we might expect the $\delta^{18}\text{O}$ and $\delta^2\text{H}$ values to converge on the $\delta^{18}\text{O}$ and $\delta^2\text{H}$
674 value of the atmosphere. For example, we might expect water vapor from the light water test to
675 have the most significant change in isotope value, towards that of the ambient atmosphere.
676 Instead, the consistency across >135 flasks, different starting water vapor isotope values, sample
677 introduction methods, and multiple analytical sessions suggests that this difference is a function
678 of the storage and measurement process. In particular, the normality of the distribution suggests
679 whatever the origin of the offset is, there is a systematic bias that we can reliably correct for.

680 **6.1.2.1 Offset correction**

681 To correct our data for this offset, we chose to use the median value as an offset
682 correction rather than the mean of the normal distribution, because the median is not biased by
683 major outlier isotope values that reflect abnormal values that go beyond analytical noise, such as
684 a slow but major leak that changes the values far beyond the basic offset seen in the dataset. The
685 calculated average offset is 1.0‰ and 2.6‰ for $\delta^{18}\text{O}$ and $\delta^2\text{H}$, respectively. After applying these
686 values as an offset correction to the data, most flasks also fall within the uncertainty of the water
687 vapor permeable probes ($\delta^{18}\text{O} = \pm 0.5\%$ and $\delta^2\text{H} = \pm 2.4\%$, Oerter et al., 2016), and the values
688 are distributed about 0 (Figs. 4C, 5C). However, the uncertainty of the SWISS system is higher
689 than that of the probes alone. Based on the results of the water vapor tests, we estimate the
690 uncertainty of the SWISS at $\pm 0.9\%$ and $\pm 3.7\%$ for $\delta^{18}\text{O}$ and $\delta^2\text{H}$, respectively using the
691 interquartile range (IQR) of the water vapor test results after removing outliers from the dataset.
692 We prefer the IQR over the calculated standard deviation of the normal distribution, because
693 IQR is not biased by outlier values. This level of uncertainty is large relative to other methods,
694 but is sufficient for many critical zone applications, given the magnitude of seasonal variability
695 in the top ~50 cm of a soil profile that can be observed in natural systems (e.g. Oerter et al.,
696 2017; Quade et al., 2019). We also expect that uncertainties will decrease with future lab-based
697 or near research facility testing and by comparing the SWISS against other soil water extraction
698 methods.

700 The relationship between $\delta^2\text{H}$ values and $\delta^{18}\text{O}$ values in a dual-isotope plot provides
701 insight into the mechanism driving the offset. Without an offset correction applied, the slope of
702 the relationship between $\delta^2\text{H}$ and $\delta^{18}\text{O}$ is 3.14 ($R^2 = 0.62$) (Supplemental Fig. 4). This slope is
703 only slightly higher than evaporation under pure diffusion (Gonfiantini et al., 2018). This
704 suggests that the offset is likely driven by diffusion and will likely vary according to climate of
705 the lab. For example, in a dry climate like Colorado, the water vapor concentration in the flask is
706 significantly higher than the atmosphere, creating a larger diffusive gradient potential than for a
707 lab in a more humid climate. We therefore strongly encourage future users to test their SWISS
708 under climate conditions similar for their applications. Further, we encourage users who might

709 use the SWISS as part of a tracer study that uses labeled heavy water to test the SWISS with
710 labeled waters prior to their field experiments to verify reliability.

711

712 *6.1.2.2 Comparing sample introduction methods*

713 Supplemental figure 6 shows a kernel density estimate plot of the results from two water
714 vapor test sessions, with the offset correction applied. During the March 2022 session, flasks
715 were measured using the dead-end pull sample introduction method and during the August 2022
716 session, flasks were measured using the dry air carrier gas sample introduction method. There is
717 no significant difference in the measured difference between the two sample introduction
718 methods. That said, we prefer the dry air carrier gas method, because it is far simpler to control
719 the water vapor mixing ratio, and optimize the concentration to be around 25,000 ppm, which is
720 the concentration at which the Picarro L2130-*i* is most reliable. The dry air carrier gas method
721 also makes it easier to control for and monitor for condensation in the stainless-steel tubing and
722 vapor impermeable tubing, which can bias a measurement.

723

724 *6.1.3 Field suitability tests*

725 The long dry air tests in the field are a useful complement to the shorter in-lab tests
726 because they test the reliability of the system at field-deployment timescales. It is clear from the
727 34 and 43 day tests that the flasks are reasonably resistant to leaks on the timescale of a normal
728 four – six week deployment (Fig. 6A). These tests also give us confidence that flasks filled later
729 in the sampling sequence do not take on an atmospheric signal prior to sampling. There are a few
730 possibilities to explain the poorer performance of the Toblerone SWISS unit during the 52-day
731 test. (Fig. 6A). The first is that there is a real threshold past which the SWISS are no longer able
732 to retain samples. However, this explanation would suggest that there should be a gradual
733 decrease in performance across the three tests, which we do not observe. The alternative
734 explanation is that the poor performance is a result of inter-unit variability. The 52-day test was
735 the first long-term test and was performed in August 2021. In August 2021, we were continuing
736 to build new SWISS units and continuing to learn from each successive round of QA/QC, so it
737 seems plausible that there were unidentified problems with the SWISS unit Toblerone that were
738 solved before the water vapor tests in August 2022.

739 In figure 6B, the data show that the flasks preserved the $\delta^{18}\text{O}$ value of both flash-
740 evaporated and atmospheric water vapor over a seven-day period. One flask was removed from
741 the dataset (flask eight), because there was visible condensation in the clear impermeable tubing
742 during the measurement phase, with an increase of $> 5\%$ for $\delta^{18}\text{O}$ during the measurement
743 period. The condensation appeared as small (< 1 mm) bubbles of water all along the impermeable
744 tubing, but the bubbles were concentrated near the connection between the SWISS and the
745 impermeable tubing. Notably, the two flasks whose $\delta^{18}\text{O}$ values do not overlap within
746 uncertainty are more negative than expected, rather than drifting towards atmospheric values or
747 values expected from diffusive fractionation. In contrast to the $\delta^{18}\text{O}$ values, only three flasks
748 filled with flash evaporated water vapor overlap within uncertainty of the known $\delta^2\text{H}$ values,
749 while four of the five flasks overlap within uncertainty of the estimated atmosphere isotope
750 value. The flasks tend to drift towards the value of the atmosphere, but retain the overall data
751 pattern from the oxygen isotope values.

752 The relatively high failure rate of this ‘mock’ field test was somewhat surprising given
753 the results of the water vapor tests done in the laboratory. Going into the test, we suspected that
754 flasks six and eight were slightly leaky based on previous water vapor tests; these were flasks

755 that previously performed poorly, but did not ‘fail’ during the water vapor test. Once we
756 collected the data, we compared the data for flasks six and eight to other flasks in the sequence.
757 During the measurement of flask eight, we observed condensation in the sample introduction
758 lines, and because the isotope values were so different relative to other flasks, we felt confident
759 in our exclusion of flask eight. Flask six had $\delta^{18}\text{O}$ and $\delta^2\text{H}$ values similar to others from the same
760 sampling source, and seemed to fall within the pattern as expected. Therefore, we chose to keep
761 this data point in the dataset.

762 We hypothesize that one major problem with the mock field test dataset was the creation
763 of condensation in the sampling lines, as others have experienced in their setups (e.g. Quade et
764 al., 2019; Kühnhammer et al., 2019). Of particular interest are the flasks that had a lower than
765 expected $\delta^{18}\text{O}$ value (flasks four and nine). It is possible that those samples were also affected by
766 condensation, but in contrast to flask eight, which was excluded because of condensation during
767 measurement, we think that these samples may have been altered because of condensation at the
768 sampling stage. During condensation, we expect that ^{18}O will preferentially enter the liquid
769 phase, and that the water vapor that enters the flask will have a lower than expected $\delta^{18}\text{O}$ value.
770 The unique advantage of the SWISS is that it can operate independently, but with that comes the
771 trade-off that we cannot currently observe condensation in the lines during sample collection. To
772 prevent condensation from forming, other users have warmed the impermeable tubing between
773 the probes and the Picarro instrument. The ‘mock’ field test data suggest that in many situations
774 it may be worthwhile to warm the transfer tubing, but this should be done in a way that does not
775 alter the thermal structure of the soil, and in remote settings, can operate safely independently.
776

777 ***6.1.4 Lessons learned and recommendations from the QA/QC and field suitability tests:***

778 Our QA/QC process was a relatively efficient way to test the soundness of the SWISS
779 units. Through the QA/QC process we were able to identify problems with units, and
780 appropriately address them before deploying units to the field. We strongly recommend that any
781 user deploying SWISS to the field to undertake the same, or similar, QA/QC process.

782 The dry air test is a time-efficient and low-cost method for identifying flasks that are
783 leaky and will not preserve the sampled water vapor isotope values. It is useful during the
784 building stage to identify fittings that need to be tightened or flasks that need to be replaced, and
785 therefore we recommend these tests as a required pre-deployment step for future SWISS units.
786 We found that it was most time and energy efficient to move onto the next level of QA/QC once
787 13 out of 15 flasks of a SWISS unit had passed the dry-air test, because frequently the remaining
788 two flasks still had relatively low water vapor mole fractions (i.e. 500 – 700 ppm), and we could
789 sufficiently tighten the fittings prior to the start of the water vapor tests for them to be successful.
790 The dry air test is a low time and expense burden that can also be used to monitor SWISS units
791 for normal wear-and-tear (e.g. a flask that cracked during transport) during deployment periods.
792 Therefore, to ensure that SWISS units continue to operate as expected, we also recommend that
793 dry air tests be done between field deployments on every SWISS unit. Lastly, we note that the
794 dry air test could be modified based on available equipment (for example, if an instrument is
795 available to measure trace atmospheric gases, that could be used instead).

796 Based on the results of the long, field dry air test, we recommend that the water vapor
797 storage time doesn’t exceed 40 days for reliable results, or that the user undertake multiple dry
798 air tests with either lower concentration benchmarks or longer duration if deployments may
799 exceed 40 days.

800 Overall, the quality control and quality assurance as well as the field suitability tests
801 demonstrate that the SWISS units can retain the isotope values of water vapor collected using
802 water vapor permeable probes. Like many other systems that measure dual isotopes (i.e. $\delta^{18}\text{O}$
803 and $\delta^2\text{H}$), each system must be evaluated separately. In general, we interpret oxygen isotope data
804 with a higher degree of confidence than the hydrogen isotope data. As the automation test
805 revealed however, even when the absolute $\delta^2\text{H}$ value is not correct, the general pattern can reveal
806 information about soil water dynamics.

807 Finally, we opted to use a large flask volume because we hypothesize that it allows us to
808 measure a sample for long enough on a CRDS that we get reliable data, without interacting with
809 vapor bound to the flask walls. The drawback of this, however, is that we must sample soil water
810 vapor for a relatively long period of time (45 minutes). In supplemental figure 7, we show that
811 the sampling regime, and particularly the length of time we pump dry air through the tubing,
812 does not significantly alter the soil moisture content of the soil. Additionally, we demonstrate
813 that the sampling regime we use does not introduce significant memory effects.

814

815 **6.2 Field Deployments**

816 In Figure 7 we show the results of three field deployments completed during summer
817 2022 (Table 3). At the Oglala National Grassland site, we used the SWISS unit named Lindt to
818 collect samples. During the August 2022 water vapor test on Lindt, all $\delta^{18}\text{O}$ values fall within
819 uncertainty of the system, and nine of the fifteen $\delta^2\text{H}$ values fall within uncertainty of the system.
820 Therefore, we interpret the $\delta^{18}\text{O}$ values with greater confidence and the $\delta^2\text{H}$ values with lower
821 confidence (Figs. 4C and 5C). We note that the $\delta^{18}\text{O}$ and $\delta^2\text{H}$ values broadly follow the same
822 trends, and fall on the global meteoric water line (Figs. 7 and 8A). In general, soil water from 25
823 cm had higher $\delta^{18}\text{O}$ and $\delta^2\text{H}$ values than soil water from both 50 and 75 cm (Fig. 8A). Given that
824 4 of the 5 samples from 25 cm overlap with the GMWL and have a d-excess that overlaps with
825 $10 \pm 2.6\text{‰}$, the soil water from that depth may reflect summer precipitation with higher $\delta^{18}\text{O}$ and
826 $\delta^2\text{H}$ values. Soil water from 75 cm had intermediate $\delta^{18}\text{O}$ and $\delta^2\text{H}$ values for most of the study
827 period, and soil water from 50 cm depth had the lowest $\delta^{18}\text{O}$ and $\delta^2\text{H}$ values for most of the
828 study period, which may reflect a more mean-annual or winter precipitation biased value. Based
829 on data available from the National Weather Service (Chadron, NE), there were likely significant
830 precipitation events on 2022-06-25 and 2022-07-08 at the field site. There is a significant shift to
831 lower $\delta^{18}\text{O}$ values at a sampling depth of 25 cm between 2022-06-25 and 2022-06-29, as well as
832 a marked increase in the d-excess value (Fig. 8A). We interpret this shift as infiltration of
833 precipitation with lower $\delta^{18}\text{O}$ values, which is supported by a return of d-excess values to $\sim 10\text{‰}$
834 (Fig. 8A). The National Weather Service reported 21.33 mm (0.84 inches) of rain at Chadron
835 Municipal Airport, approximately 50 km from the study site on 2022-07-08, which likely was
836 associated with at least some precipitation at our field site. Following the significant rain event
837 on 2022-07-08, we observe a marked increase in the stable isotope value of water vapor from a
838 sampling depth of 50 cm, towards values that are much closer to those at 25 cm depth. These
839 data suggests that soil water isotopes at 50 cm in this silt-loam Aridisol may be fairly sensitive to
840 large individual precipitation events, while at 75 cm soil water isotopes remain comparatively
841 uniform. Future work should address how drought conditions, storm size, pore size distribution,
842 and soil clay mineralogy influence the variability of soil water isotopes with depth.

843 At Briggsdale, CO we used the SWISS named Raclette to collect soil water vapor
844 samples. Data from 25 cm depth at Briggsdale, CO were discarded because the water vapor mole
845 fraction was much lower than would be expected given the soil temperature (i.e. $< 15,000$ ppm).

846 The gravimetric water concentration (GWC) at that soil depth at the time of sampling was
847 approximately 4% through the sampling period. Future work should include a multiple-method
848 (e.g. cryogenic extraction, centrifugation, etc.) comparison of soil water isotopes at low water
849 contents to better understand what these samples might represent, and if they are actually
850 representative of soil conditions.

851 Based on the results of the August 2022 water vapor test done on Raclette where all
852 flasks fell within uncertainty of the SWISS system for both $\delta^{18}\text{O}$ and $\delta^2\text{H}$, except for flask 11
853 (Figs. 4C and 5C), we interpret all data with greater confidence. Flask 11 corresponds to the 25
854 cm depth sample from 2022-07-27, and was already culled from the dataset because of low water
855 vapor mole fraction associated with the very dry soil. The soil water $\delta^{18}\text{O}$ and $\delta^2\text{H}$ values from a
856 sampling depth of 50 cm and 75 cm overlap within uncertainty, but the soil water $\delta^{18}\text{O}$ and $\delta^2\text{H}$
857 values from 50 cm are higher than the isotope values from 75 cm. All of the data from each
858 sampling depth group (i.e. 50 cm and 75 cm) overlap within uncertainty, conforming to the
859 expectation that soil water from these sampling depths should be fairly invariant (e.g. Oerter et
860 al., 2019). There were precipitation events at the study site on 2022-07-24, 2022-07-28 and
861 2022-07-31. It is possible that the slight negative shift in both $\delta^{18}\text{O}$ and $\delta^2\text{H}$ on 2022-08-01
862 reflects infiltration of precipitation to those depths, but this is not certain given that all of the
863 measurements from within a sampling depth overlap within uncertainty.

864 At Seibert, CO we used the SWISS named Toblerone to collect soil water vapor samples.
865 The soil water isotope data from 75 cm depth at this site offer a few useful lessons for future
866 users. The two key observations of the data from 75 cm depth are that the $\delta^{18}\text{O}$ and $\delta^2\text{H}$ values
867 are much higher than the ones from other two sampling depths, and that the $\delta^2\text{H}$ and $\delta^{18}\text{O}$ values
868 do not move in parallel with each other. While measuring these samples we observed
869 condensation in the impermeable tubing at the point where the SWISS connects to the
870 impermeable tubing. Additionally, when we heated the stainless-steel tubing that connects the
871 tubing flask and Valco valve we observed a rapid increase in water vapor mole fraction (1000's
872 of ppm over <30 seconds) that was accompanied by a rise in stable isotope value. During these
873 measurements, we were rarely able to get a stable isotope value measurement window, and
874 instead the stable isotope value of the vapor increased continually through the measurement. It is
875 for these reasons that we feel confident in discarding the stable isotope data from 2022-06-19 –
876 2022-06-29. The final measurement from 75 cm depth on 2022-07-04 approaches a reasonable
877 isotope value when compared to isotope values from the other two depths, and that sample had
878 fewer condensation problems during measurement. However, because we have no sequential
879 context for what a reasonable value for this depth is, we discarded that value as well. For that
880 final 75 cm sample, we were more successful because we warmed the entire length the vapor
881 impermeable tubing, as well as the stainless-steel tubing, flask, and Valco valve evenly so that
882 there were no temperature gradients across the vapor path. If the condensation had only been in
883 the impermeable tubing it would have been much easier to successfully analyze these samples by
884 just closing off the flask and running dry air through the tubing to remove condensation, but
885 because condensation was also occurring in the stainless-steel tubing between the flask and
886 Valco valve, this was not possible. It remains unclear why condensation was such a significant
887 problem for samples from that depth as opposed to samples from different depths in the same
888 SWISS. Future work should include further testing of the SWISS across different water contents
889 and temperatures to better understand why the phenomenon may have occurred.

890 Based on the results of the August 2022 water vapor test done on Toblerone, we interpret
891 all data from 50 cm and 25 cm depth with high confidence, except for Flask 3, which is the 50

892 cm sample from 2022-06-19 (Figs. 4C and 5C). Unlike data from the other two field sites, soil
893 water from 25 cm and 50 cm overlap within uncertainty. There were two precipitation events at
894 the field site during the sampling period on 2022-06-25 and 2022-07-01, but both events were
895 quite small (<0.5 mm, CoAgMet). There is no significant influence of the precipitation events on
896 the $\delta^{18}\text{O}$ and $\delta^2\text{H}$ values. The >1.0‰ increase in $\delta^{18}\text{O}$ values on 2022-06-29 is surprising given
897 that there is not a comparable magnitude increase in $\delta^2\text{H}$ value, and that the values measured
898 from 2022-07-04 more closely match the $\delta^{18}\text{O}$ and $\delta^2\text{H}$ values from the two earlier sampling
899 days. There are two potential explanations for this data. First, that this shift is a real signal from
900 an evaporation driven increase in the $\delta^{18}\text{O}$ value, and the shift back to a lower $\delta^{18}\text{O}$ value on
901 2022-07-04 is due to the infiltration of precipitation, which could also explain the low d-excess
902 value associated with this measurement (Supplemental Fig. 8). The second possible explanation
903 is that the 25 cm sample from 2022-06-29 is influenced by condensation at the time of sampling.
904 Dew point at the field site on 2022-06-29 significantly decreased as compared to the other
905 sampling days to a monthly minimum of 20.6°C (CoAgMet). It is possible that environmental
906 conditions encouraged the formation of condensation in the impermeable tubing at the time of
907 sampling; if there was residual condensation in the impermeable tubing then its possible we
908 were partially sampling a heavier condensed water. There were no obvious signs of condensation
909 during the time of measurement in the lab. These results highlight the utility of having broad
910 contextual environmental data to aid in the interpretation of soil water isotope data.

911 All together, these three soil water isotope datasets demonstrate two main findings. First,
912 data from these samples show that the differences between field sites are easily resolvable using
913 the SWISS. For example, at 50 cm depth the oxygen isotopes range between -14.4 to -16.3‰, -
914 9.9 to -10.3‰, and -7.4 to -9.3‰ for the Oglala, Briggsdale and Seibert sites, respectively. These
915 differences likely reflect differences in the stable isotope composition of precipitation and
916 infiltration and evaporation dynamics. Second, the sample data retrieved from a SWISS are
917 sufficiently precise to be able to meaningfully resolve vertical profile soil water isotope data. For
918 example, at the Oglala National Grassland field site, soil water from 25 cm clearly has higher
919 $\delta^{18}\text{O}$ and $\delta^2\text{H}$ values as compared to soil water from a depth of 50 and 75 cm.

920

921 **6. 3 Future improvements and future work**

922 One significant SWISS unit hardware improvement that could be made would be to
923 install a heating implement to the flasks. One source of uncertainty on the current system is the
924 potential effect of uneven heating of the flasks prior to measurement which may create
925 temperature gradients that are large enough to allow for condensation when warm vapor meets a
926 spot slightly colder than dew point. This could be improved in subsequent iterations of the
927 SWISS with the addition of heat tape or blankets that can deliver controlled heat and create
928 consistent temperatures. This improvement would also help limit the amount of manual
929 intervention needed during measurement, and could improve automation of flask measurement.
930 Additionally, finding a way to safely and automatically heat the impermeable tubing that
931 connects the water vapor probes and the SWISS in a way that doesn't change the inherent
932 thermal structure of the soil, and is safe for unmonitored use, would help to prevent the
933 formation of condensation in the field and reduce the uncertainties related to sampling as well as
934 the number of samples that need to be discarded.

935 We have made a few improvements to the automation system that were not implemented
936 for the data presented in this contribution, but will be part of future deployments. First, we will
937 track conditions inside the SWISS with a temperature and relative humidity sensor inside the

938 case. Second, we plan to eliminate the power inverter by powering both the Valco valve and
939 mass flow controller with VDC using a power step up controller. Lastly, we will add an IoT
940 cellular router to be able to remotely monitor and control the SWISS units. This would be
941 particularly helpful if there is a sampling day that is unexpectedly cold or when the dew point at
942 the field site is unexpectedly low and we expect condensation to form more readily in the field,
943 or if there is a precipitation event that we are interested in capturing, because with the IoT
944 cellular router we could remotely alter the sampling plan.

945 While the improvements and additional testing we have done to the SWISS in this
946 contribution represent a significant step forward, additional work should be done to make the
947 system more useable by the ecohydrology community. We have rigorously tested the SWISS in
948 the lab, and demonstrated a few ways in which the SWISS can fail in field settings. A full
949 comparison of how soil water isotope data collected using a SWISS as compared to other in situ
950 (both vapor probes and lysimeter) and destructive sampling methods would shed more light on
951 the accuracy and precision of our system, and the applicability of our lab-based experiments to
952 the field. These experiments should be carefully designed with considerations of soil grain size,
953 soil water content, expected isotope values, and climate. Additionally, we plan to test SWISS
954 unit resilience during air travel so that these units can be used at field sites that are not within
955 driving distance of a research facility.

956 **Conclusions**

957 We presented the evolution of the soil water isotope storage system (SWISS) from a
958 prototype to a fully built out and tested system. We also presented a quality control and quality
959 assurance procedure that we strongly recommend future users undertake to ensure the reliable
960 storage of soil water vapor over long time periods (up to 40 days). In addition, these quality
961 control and quality assurance tests shed light on the accuracy and precision of the SWISS. After
962 applying an offset correction, we determined the precision of the SWISS to be $\pm 0.9\%$ and
963 $\pm 3.7\%$ for $\delta^{18}\text{O}$ and $\delta^2\text{H}$, respectively. In a field setting, flasks reliably resist atmospheric
964 intrusion. Additionally, the proposed sampling schema does not introduce significant memory
965 effects. Lastly, we demonstrated that the current precision of the SWISS still allows us to
966 distinguish between field sites and between soil water dynamics within a single soil column.
967 Taken as a whole, these data show that the SWISS can be used as a tool to answer many
968 emerging ecohydrological questions, and will enhance researchers' ability to collect soil water
969 isotope datasets from more remote and traditionally understudied field sites.

970 **Acknowledgements**

971 We thank the numerous field assistants who helped to make the field work presented in
972 this paper possible, including Spencer Burns, Anne Fetrow, Sarah Brookins, Juliana Olsen-
973 Valdez, and Haley Brumberger. We acknowledge that both field work and laboratory work for
974 this study were done on the traditional territories and ancestral homelands of the Arapahoe, Ute
975 and Cheyenne peoples. This work was supported by startup funding from CU Boulder and NSF
976 funding from grant EAR-2023385 awarded to K. Snell. Additionally, this work was supported by
977 the University of Colorado Boulder Beverly Sears Research Grant and the Clay Minerals Society
978 Graduate Student Research Grant both awarded to R. Havranek. CUBES-SIL is a CU Boulder
979 Core Facility associated with RRID: SCR_019300.

980

981 **Author contribution**

982 Rachel E. Havranek: conceptualization, methodology, investigation, formal analysis, funding
983 acquisition, writing – wrote original draft, review and editing. Kathryn E. Snell:

984 conceptualization, methodology, writing – review & editing, funding acquisition. Sebastian H.

985 Kopf: conceptualization, methodology, writing – review & editing. Brett Davidheiser-Kroll:

986 conceptualization, methodology, writing – review & editing. Valerie Morris: methodology,

987 writing – review & editing. Bruce Vaugh: methodology, writing – review & editing.

988

989 **Competing interests**

990 The authors declare no competing interests.

991 **Works Cited**

- 992 Beyer, M., Kühnhammer, K., & Dubbert, M.: In situ measurements of soil and plant water
993 isotopes: a review of approaches, practical considerations and a vision for the future.
994 Hydrology and Earth System Sciences, 24, 4413–4440
995 <https://doi.org/https://doi.org/10.5194/hess-24-4413-2020>, 2020.
- 996 Bowen, G. J., Cai, Z., Fiorella, R. P., & Putman, A. L.: Isotopes in the Water Cycle: Regional- to
997 Global-Scale Patterns and Applications. Annual Review of Earth and Planetary Sciences,
998 47(1), 453–479, <https://doi.org/10.1146/annurev-earth-053018-060220>, 2019
- 999 Bowen, G. J., Putman, A., Brooks, J. R., Bowling, D. R., Oerter, E. J., & Good, S. P.: Inferring
1000 the source of evaporated waters using stable H and O isotopes. Oecologia, 187(4), 1025–
1001 1039, <https://doi.org/10.1007/s00442-018-4192-5>, 2018.
- 1002 Brooks, J. R., Barnard, H. R., Coulombe, R., & McDonnell, J. J.: Ecohydrologic separation of
1003 water between trees and streams in a Mediterranean climate. Nature Geoscience, 3(2), 100–
1004 104, <https://doi.org/10.1038/ngeo722>, 2010.
- 1005 CoAgMet, Colorado Climate Center, Colorado State University, Fort Collins, CO, USA.
1006 <https://coagmet.colostate.edu/>, last access: 25 April 2023.
- 1007 Dawson, T. E., & Ehleringer, J. R.: Streamside trees that do not use stream-water: evidence from
1008 hydrogen isotopes ratios. Nature, 350(March), 335–337, <https://doi.org/10.1038/350335a0>,
1009 1991.
- 1010 Gaj, M., Beyer, M., Koeniger, P., Wanke, H., Hamutoko, J., & Himmelsbach, T.: In-situ
1011 unsaturated zone stable water isotope (^2H and ^{18}O) measurements in semi-arid environments
1012 using tunable off-axis integrated cavity output spectroscopy. Hydrology and Earth System
1013 Sciences Discussions, 12(6), 6115–6149, <https://doi.org/10.5194/hessd-12-6115-2015>, 2015
- 1014 Gaj, M., Beyer, M., Koeniger, P., Wanke, H., Hamutoko, J., & Himmelsbach, T.: In situ
1015 unsaturated zone water stable isotope (^2H and ^{18}O) measurements in semi-arid
1016 environments: A soil water balance. Hydrology and Earth System Sciences, 20(2), 715–731.
1017 <https://doi.org/10.5194/hess-20-715-2016>, 2016.
- 1018 Gessler, A., Bächli, L., Rouholahnejad Freund, E., Treydte, K., Schaub, M., Haeni, M., Weiler,
1019 M., Seeger, S., Marshall, J., Hug, C., Zweifel, R., Hagedorn, F., Rigling, A., Saurer, M., &
1020 Meusburger, K.: Drought reduces water uptake in beech from the drying topsoil, but no
1021 compensatory uptake occurs from deeper soil layers. New Phytologist, 233(1), 194–206,
1022 <https://doi.org/10.1111/nph.17767>, 2022.
- 1023 Gómez-Navarro, C., Pataki, D. E., Bowen, G. J., & Oerter, E. J.: Spatiotemporal variability in
1024 water sources of urban soils and trees in the semiarid, irrigated Salt Lake Valley.
1025 Ecohydrology, 12(8), <https://doi.org/10.1002/eco.2154>, 2019.
- 1026 Gonfiantini, R., Wassenaar, L. I., Araguas-Araguas, L., & Aggarwal, P. K.: A unified Craig-
1027 Gordon isotope model of stable hydrogen and oxygen isotope fractionation during fresh or
1028 saltwater evaporation, Geochimica et Cosmochimica Acta, 235, 224–236.
1029 <https://doi.org/10.1016/j.gca.2018.05.020>, 2018.
- 1030 Good, S. P., Noone, D., & Bowen, G. J.: Hydrologic connectivity constrains partitioning of
1031 global terrestrial water fluxes. Science, 349(6244), 175–177,
1032 <https://doi.org/10.1126/science.aaa5931>, 2015.

- 1033 Green, M. B., Laursen, B. K., Campbell, J. L., McGuire, K. J., & Kelsey, E. P.: Stable water
 1034 isotopes suggest sub-canopy water recycling in a northern forested catchment. *Hydrological*
 1035 *Processes*, 29(25), 5193–5202, <https://doi.org/10.1002/hyp.10706>, 2015
- 1036 Groh, J., Stumpp, C., Lücke, A., Pütz, T., Vanderborght, J. and Vereecken, H.: Inverse
 1037 estimation of soil hydraulic and transport parameters of layered soils from water stable
 1038 isotope and lysimeter data. *Vadose Zone Journal*, 17(1), 1-19,
 1039 <https://doi.org/10.2136/vzj2017.09.0168>, 2018.
- 1040 Gupta, P., Noone, D., Galewsky, J., Sweeney, C., and Vaughn, B.H.: Demonstration of high-
 1041 precision continuous measurements of water vapor isotopologues in laboratory and remote
 1042 field deployments using wavelength-scanned cavity ring-down spectroscopy (WS-CRDS)
 1043 technology. *Rapid Com. in Mass Spectrometry*, 23, 2534-2542,
 1044 <https://doi.org/10.1002/rcm.4100>, 2009
- 1045 Harms Sarah M, & Ludwig, T. K.: Retention and removal of nitrogen and phosphorus in saturated
 1046 soils of arctic hillslopes. *Biogeochemistry*, 127, 291–304 [https://doi.org/10.1007/s10533-](https://doi.org/10.1007/s10533-016-0181-0)
 1047 [016-0181-0](https://doi.org/10.1007/s10533-016-0181-0), 2016.
- 1048 Havranek, R. E., Snell, K. E., Davidheiser-Kroll, B., Bowen, G. J., & Vaughn, B.: The Soil
 1049 Water Isotope Storage System (SWISS): An integrated soil water vapor sampling and
 1050 multiport storage system for stable isotope geochemistry. *Rapid Communications in Mass*
 1051 *Spectrometry*, 34(12), 1–11. <https://doi.org/10.1002/rcm.8783>, 2020
- 1052 Hinckley, E.-L. S., Barnes, R. T., Anderson, S. P., Williams, M. W., & Bernasconi, S. M.:
 1053 Nitrogen retention and transport differ by hillslope aspect at the rain-snow transition of the
 1054 Colorado Front Range. *Journal of Geophysical Research: Biogeosciences*, 119, 12811896.
 1055 <https://doi.org/10.1002/2013JG002588>, 2014.
- 1056 Kübert, A., Paulus, S., Dahlmann, A., Werner, C., Rothfuss, Y., Orłowski, N., & Dubbert, M. :
 1057 Water Stable Isotopes in Ecohydrological Field Research : Comparison Between In Situ and
 1058 Destructive Monitoring Methods to Determine Soil Water Isotopic Signatures. *Frontiers in*
 1059 *Plant Science*, 11(April), 1–13, <https://doi.org/10.3389/fpls.2020.00387>, 2020.
- 1060 Kühnhammer, K., Dahlmann, A., Iraheta, A., Gerchow, M., Birkel, C., Marshall, J. D., & Beyer,
 1061 M.: Continuous in situ measurements of water stable isotopes in soils, tree trunk and root
 1062 xylem: Field approval. *Rapid Comm. in Mass Spec.*, 36(5).
 1063 <https://doi.org/10.1002/rcm.9232>, 2022.
- 1064 Magh, R.K., Gralher, B., Herbstritt, B., Kübert, A., Lim, H., Lundmark, T. and Marshall, J.:
 1065 Technical note: Conservative storage of water vapour–practical in situ sampling of stable
 1066 isotopes in tree stems, *Hydrol. Earth Syst. Sci.*, 26, 3573–3587, [https://doi.org/10.5194/hess-](https://doi.org/10.5194/hess-26-3573-2022)
 1067 [26-3573-2022](https://doi.org/10.5194/hess-26-3573-2022), 2022.
- 1068 Mahindawansa, A., Orłowski, N., Kraft, P., Rothfuss, Y., Racela, H., & Breuer, L.:
 1069 Quantification of plant water uptake by water stable isotopes in rice paddy systems. *Plant*
 1070 *and Soil*, 429(1–2), 281–302. <https://doi.org/10.1007/s11104-018-3693-7>, 2018
- 1071 Oerter, E. J., Perelet, A., Pardyjak, E., & Bowen, G. J.: Membrane inlet laser spectroscopy to
 1072 measure H and O stable isotope compositions of soil and sediment pore water with high
 1073 sample throughput. *Rapid Communications in Mass Spectrometry*, 31(1), 75–84,
 1074 <https://doi.org/10.1002/rcm.7768>, 2016.

- 1075 Oerter, E. J., & Bowen, G. J.: In situ monitoring of H and O stable isotopes in soil water reveals
 1076 ecohydrologic dynamics in managed soil systems. *Ecohydrology*, 10(4), 1–13,
 1077 <https://doi.org/10.1002/eco.1841>, 2017
- 1078 Oerter, E. J., & Bowen, G. J.: Spatio-temporal heterogeneity in soil water stable isotopic
 1079 composition and its ecohydrologic implications in semiarid ecosystems. *Hydrological*
 1080 *Processes*, March, 1–15. <https://doi.org/10.1002/hyp.13434>, 2019
- 1081 Peterson, B. J., & Fry, B.: Stable Isotopes in Ecosystem Studies. *Annual Reviews of Ecology and*
 1082 *Systematics*, 18, 293–320, <http://www.jstor.org/stable/2097134>, 1987.
- 1083 Quade, M., Klosterhalfen, A., Graf, A., Brüggemann, N., Hermes, N., Vereecken, H., &
 1084 Rothfuss, Y.: In-situ monitoring of soil water isotopic composition for partitioning of
 1085 evapotranspiration during one growing season of sugar beet (*Beta vulgaris*). *Agri. and*
 1086 *Forest Met.*, 266–267, 53–64. <https://doi.org/10.1016/j.agrformet.2018.12.002>, 2019.
- 1087 Quade, M., Brüggemann, N., Graf, A., Vanderborght, J., Vereecken, H., & Rothfuss, Y.:
 1088 Investigation of Kinetic Isotopic Fractionation of Water during Bare Soil Evaporation.
 1089 *Water Resources Research*, 54(9), 6909–6928, <https://doi.org/10.1029/2018WR023159>,
 1090 2018.
- 1091 Rothfuss, Y., Vereecken, H., & Brüggemann, N.: Monitoring water stable isotopic composition
 1092 in soils using gas-permeable tubing and infrared laser absorption spectroscopy. *Water*
 1093 *Resources Research*, 49, 3747–3755, <https://doi.org/10.1002/wrcr.20311>, 2013.
- 1094 Rothfuss, Y., Merz, S., Vanderborght, J., Hermes, N., Weuthen, A., Pohlmeier, A., Vereecken,
 1095 H., & Brüggemann, N.: Long-term and high-frequency non-destructive monitoring of water
 1096 stable isotope profiles in an evaporating soil column. *Hydrol. Earth Syst. Sci.*, 19(10),
 1097 4067–4080, <https://doi.org/10.5194/hess-19-4067-2015>, 2015.
- 1098 Rothfuss, Y., Quade, M., Brüggemann, N., Graf, A., Vereecken, H., & Dubbert, M.: Reviews
 1099 and syntheses: Gaining insights into evapotranspiration partitioning with novel isotopic
 1100 monitoring methods., *Biogeosciences*, 18 (12), 3701–3732, [https://doi.org/10.5194/bg-18-](https://doi.org/10.5194/bg-18-3701-2021)
 1101 [3701-2021](https://doi.org/10.5194/bg-18-3701-2021), 2021.
- 1102 Rozmiarek, K. S., Vaughn, B. H., Jones, T. R., Morris, V., Skorski, W. B., Hughes, A. G.,
 1103 Elston, J., Wahl, S., Faber, A. K., & Steen-Larsen, H. C.: An unmanned aerial vehicle
 1104 sampling platform for atmospheric water vapor isotopes in polar environments.
 1105 *Atmospheric Measurement Techniques*, 14(11), 7045–7067, [https://doi.org/10.5194/amt-14-](https://doi.org/10.5194/amt-14-7045-2021)
 1106 [7045-2021](https://doi.org/10.5194/amt-14-7045-2021), 2021.
- 1107 Seeger, S., & Weiler, M.: Temporal dynamics of tree xylem water isotopes: In situ monitoring
 1108 and modeling. *Biogeosciences*, 18(15), 4603–4627, [https://doi.org/10.5194/bg-18-4603-](https://doi.org/10.5194/bg-18-4603-2021)
 1109 [2021](https://doi.org/10.5194/bg-18-4603-2021), 2021.
- 1110 Soderberg, K., Good, S. P., Wang, L., & Caylor, K.: Stable Isotopes of Water Vapor in the
 1111 Vadose Zone: A Review of Measurement and Modeling Techniques. *Vadose Zone Journal*,
 1112 11(3), <https://doi.org/10.2136/vzj2011.0165>, 2012.
- 1113 Soil Survey Staff, Natural Resources Conservation Service, United States Department of
 1114 Agriculture. Soil Series Classification Database. <https://websoilsurvey.nrcs.usda.gov/>.
 1115 Accessed 09 October 2022.

- 1116 Sprenger, M., Leistert, H., Gimbei, G., & Weiler, M., Illuminating hydrological processes at the
1117 soil-vegetation-atmosphere interface with water stable isotopes. *Reviews in Geophysics*, 54,
1118 674–704, <https://doi.org/10.1002/2015RG000515>, 2016.
- 1119 Sprenger, M., & Allen, S. T.: What Ecohydrologic Separation Is and Where We Can Go With It.
1120 In *Water Resources Research* (Vol. 56, Issue 7). Blackwell Publishing Ltd.
1121 <https://doi.org/10.1029/2020WR027238>, 2020.
- 1122 Stumpp, C., Stichler, W., Kandolf, M. and Šimůnek, J.: Effects of land cover and fertilization
1123 method on water flow and solute transport in five lysimeters: A long-term study using stable
1124 water isotopes. *Vadose Zone Journal*, 11(1), <https://doi.org/10.2136/vzj2011.0075>, 2012.
- 1125 Theis, D. E., Saurer, M., Blum, H., Frossard, E., & Siegwolf, R. T. W.: A portable automated
1126 system for trace gas sampling in the field and stable isotope analysis in the laboratory. *Rapid*
1127 *Communications in Mass Spectrometry*, 18(18), 2106–2112,
1128 <https://doi.org/10.1002/rcm.1596>, 2004.
- 1129 Vereecken, H., Amelung, W., Bauke, S. L., Bogaen, H., Brüggemann, N., Montzka, C.,
1130 Vanderborght, J., Bechtold, M., Blöschl, G., Carminati, A., Javaux, M., Konings, A. G.,
1131 Kusche, J., Neuweiler, I., Or, D., Steele-Dunne, S., Verhoef, A., Young, M., & Zhang, Y.:
1132 Soil hydrology in the Earth system. *Nature Reviews Earth & Environment*, 3, 573–587,
1133 <https://doi.org/10.1038/s43017-022-00324-6>, 2022.
- 1134 Volkmann, T. H. M., & Weiler, M.: Continual in situ monitoring of pore water stable isotopes in
1135 the subsurface. *Hydrology and Earth System Sciences*, 18(5), 1819–1833,
1136 <https://doi.org/10.5194/hess-18-1819-2014>, 2014.
- 1137 Volkmann, T. H. M., Haberer, K., Gessler, A., & Weiler, M., High-resolution isotope
1138 measurements resolve rapid ecohydrological dynamics at the soil-plant interface. *New*
1139 *Phytologist*, 210(3), 839–849. <https://doi.org/10.1111/nph.13868>, 2016.
- 1140 Wassenaar, L. I., Hendry, M. J., Chostner, V. L., & Lis, G. P.: High resolution pore water $\delta^2\text{H}$
1141 and $\delta^{18}\text{O}$ measurements by $\text{H}_2\text{O}_{(\text{liquid})}$ - $\text{H}_2\text{O}_{(\text{vapor})}$ equilibration laser
1142 spectroscopy. *Environmental Science and Technology*, 42(24), 9262–9267.
1143 <https://doi.org/10.1021/es802065s>, 2008.
- 1144 Zhao, P., Tang, X., Zhao, P., Wang, C. and Tang, J., 2013. Identifying the water source for
1145 subsurface flow with deuterium and oxygen-18 isotopes of soil water collected from tension
1146 lysimeters and cores. *Journal of Hydrology*, 503, 1–10,
1147 <https://doi.org/10.1016/j.jhydrol.2013.08.033>, 2013.
- 1148 Zimmermann, U., Munnich, K. O., & Roether, W.: Tracers Determine Movement of Soil
1149 Moisture and Evapotranspiration, *Science*, 152(3720), 346–347.
1150 <https://doi.org/10.1126/science.152.3720.346>, 1966.
- 1151
- 1152